Inorg. Chem. **2007**, *46*, 9678–9691

Mixed Transition Metal–Lanthanide Complexes at High Oxidation States: Heteronuclear $Ce^{IV}Mn^{IV}$ Clusters

Anastasios J. Tasiopoulos,[†,‡] Paul L. Milligan, Jr.,[§] Khalil A. Abboud,[†] Ted A. O'Brien,[§] and George Christou*[,†]

Department of Chemistry, University of Florida, Gainesville, Florida 32611-7200, and Department of Chemistry and Chemical Biology, Indiana University–Purdue University Indianapolis, Indianapolis, Indiana 46202-3274

Received May 22, 2007

The syntheses of the first mixed-metal $Ce^{IV}Mn^{IV}$ complexes are reported. $[CeMn_2O_3(O_2CMe)(NO_3)_4(H_2O)_2(bpy)_2](NO_3)$ (**1**; bpy = 2,2′-bipyridine) was obtained from the reaction of $Mn(NO_3)_2 \cdot xH_2O$ and bpy with $(NH_4)_2Ce(NO_3)_6$ in a 1:1:2 molar ratio in 25% aqueous acetic acid. The complexes $[CeMn_6O_9(O_2CR)_9(X)(H_2O)_2]^{y+}$ (R = Me, X = NO_3^-, $y = 0$ (**2**); R = Me, X = MeOH, $y = +1$ (**3**); R = Et, X = NO_3^-, $y = 0$ (**7**)) were obtained from reactions involving a $[Mn(O_2CR)_2] \cdot 4H_2O/Ce^{IV}$ ratio of ∼1:1.5 in concentrated aqueous carboxylic acid. A related reaction in less-concentrated aqueous acetic acid and in the presence of L (where L = 2-hydroxy-6-methylpyridine (mhpH), 2-pyrrolidinone (pyroH), or pyridine (py)) gave $[Ce_3Mn_2O_6(O_2CMe)_6(NO_3)_2(L)_a(H_2O)_b]$ (L = mhpH, $a = 4$, $b = 0$ (**4**); L = pyroH, $a = 2$, $b = 3$ (**5**)) and $\{\{(pyH)_3[Ce_3Mn_2O_6(O_2CMe)_{7.5}(NO_3)_3] \cdot (HO_2CMe)_{0.5} \cdot (H_2O)_2\}_2(NO_3)\}_n$ (**6**), respectively. Solid-state magnetic susceptibility (χ_M) data for compounds **1**, **4**, and **5** were fit to the theoretical $\chi_M T$ versus T expression for a $Mn^{IV}{}_2$ complex derived using the isotropic Heisenberg spin Hamiltonian ($H = -2J\hat{S}_1\hat{S}_2$) and the Van Vleck equation. The obtained fit parameters were (in the format J, g) **1**, –45.7(3) cm^{-1}, 1.95(5); **4**, –0.40(10) cm^{-1}, 2.0(1); and **5**, –0.34(10) cm^{-1}, 2.0(1), where J is the exchange interaction constant between the two Mn^{IV} ions. The data for compound **3** were fit by a matrix diagonalization method that gave $J_1 = -5.8$ cm^{-1}, $J_2 = -0.63$ cm^{-1}, $J_3 \approx 0$, and $g = 2.0(1)$, where J_1 and J_2 are the exchange interactions for the $[Mn^{IV}{}_2O_2(O_2CMe)]$ and $[Mn^{IV}{}_2O(O_2CMe)_2]$ units, respectively, and J_3 for a uniform next-nearest-neighbor interaction. Theoretical estimates of the exchange constants in compounds **1** and **3** obtained with the ZILSH method were in excellent and good agreement, respectively, with the values obtained from fits of the magnetization data. The difference for **3** is assigned to the presence of the Ce^{4+} ion, and atomic bond indices obtained from the ZILSH calculations were used to rationalize the values of the various exchange constants based on metal–ligand bond strengths.

Introduction

High oxidation state discrete or polymeric Mn or Ce oxide complexes are of relevance to a large number of areas and applications spanning inorganic, organic, biological, environmental, and industrial chemistry because of their ability to oxidize both inorganic and organic substrates.[1–8] In addition, in a biochemical context the high oxidation state tetranuclear Mn cluster that is the water oxidizing center (WOC) within the photosynthetic apparatus of green plants and cyanobacteria is responsible for the oxidation of H_2O to O_2, the source of essentially all this gas on this planet.[1,2] This has stimulated extensive efforts to model this site, and as a result, a number of Mn_4 complexes have been synthesized to model its structural and functional properties.[1] Ce^{IV}

* To whom correspondence should be addressed. Phone: +1-352-392-8314. Fax: +1-352-392-8757. E-mail: christou@chem.ufl.edu.
† University of Florida.
‡ Present address: Department of Chemistry, University of Cyprus, 1678 Nicosia, Cyprus.
§ Purdue University.

(1) (a) Nugent, J. Ed. Special Issue on Photosynthetic Water Oxidation. *Biochim. Biophys. Acta: Bioenerg.* **2001**, *1503*, 1–259. (b) Yachandra, V. K.; Sauer, K.; Klein, M. P. *Chem. Rev.* **1996**, *96*, 2927. (c) Manchanda, R.; Brudvig, G. W.; Crabtree, R. H. *Coord. Chem. Rev.* **1995**, *144*, 1.
(2) (a) Ruttinger, W.; Dismukes, C. G. *Chem. Rev.* **1997**, *97*, 1. (b) Yagi, M.; Kaneko, M. *Chem. Rev.* **2001**, *101*, 21.
(3) (a) Tasiopoulos, A. J.; Abboud, K. A.; Christou, G. *Chem. Commun.* **2003**, 580. (b) Lis, T. *Acta Crystallogr. Sect. B* **1980**, *B36*, 2042. (c) Sessoli, R.; Tsai, H.-L.; Schake, A. R.; Wang, S.; Vincent, J. B.; Folting, K.; Gatteschi, D.; Christou, G.; Hendrickson, D. N. *J. Am. Chem. Soc.* **1993**, *115*, 1804.

10.1021/ic700994p CCC: $37.00
Published on Web 10/12/2007

has also been used in homogeneous and heterogeneous catalysis by Ru complexes of water oxidation to molecular dioxygen.[2] Similarly, MnO_4^- and Ce^{IV} are commonly employed as oxidants in inorganic synthesis, such as in the formation of Mn^{III} or Mn^{IV} clusters or mixed-valent $Co^{III,IV}$ complexes.[3,4] In addition, compounds such as MnO_4^-, MnO_2, and $(NH_4)_2Ce(NO_3)_6$ have a long history as oxidizing agents for a vast variety of organic substrates.[5,6] Further, Mn^{III}, Mn^{IV}, and Ce^{IV} oxides have been widely used, either alone or as mixed Mn/Ce oxides, in a number of heterogeneous catalytic oxidation processes.[7,8] For example, Ce^{IV}/Mn^{IV} composite oxides are widely used in sub- and supercritical catalytic wet oxidations for the treatment of wastewater containing toxic organic and inorganic pollutants such as ammonia, acetic acid, pyridine, phenol, polyethylene-glycol, and others.[8]

Given the above, it is perhaps surprising that there have not been any mixed Ce^{IV}/Mn^{IV} molecular analogues of these Ce/Mn oxide catalysts available for study. Such mixed-metal and mixed 3d/4f species would be of some structural interest, as well as likely proving to have interesting oxidative and other properties. We have therefore been developing synthetic methods for such mixed-metal species and can report the successful synthesis of a variety of products of this kind. We herein describe the synthesis and crystallographic characterization of a family of mixed Ce^{IV}/Mn^{IV} complexes, both discrete and polymeric, containing various Ce/Mn ratios. These and the related $CeMn^{III}_8$ complex reported elsewhere[9a] were the first crystallographically characterized molecular Ce/Mn complexes of any type. The magnetic properties of the complexes have been investigated experimentally and with theoretical calculations. Portions of this work have been previously communicated.[9b]

Experimental Section

Syntheses. All manipulations were performed under aerobic conditions with the use of materials as received; the water was distilled in-house. ***Caution!*** *Perchloric acid and its salts are potentially explosive and should be handled with care*. Elemental analyses were performed by Atlantic Microlab, Inc. (Norcross, GA), and at the in-house facilities of the University of Florida Chemistry Department.

$[CeMn_2O_3(O_2CMe)(NO_3)_4(H_2O)_2(bpy)_2](NO_3)$ (1). To a stirred pale yellow-brown solution of $Mn(NO_3)_2{\cdot}xH_2O$ (0.90 g, 5.0 mmol) and bpy (0.78 g, 5.0 mmol) in H_2O/HO_2CMe (50/15 mL) was slowly added an orange solution of $(NH_4)_2[Ce(NO_3)_6]$ (5.5 g, 10.0 mmol) in H_2O/HO_2CMe (19/6 mL), resulting in a dark greenish-brown solution. The volume of the solution was reduced by ∼60% by rotary-evaporation at 40 °C, and then the solution maintained undisturbed at ambient temperature. After 24 h, dark greenish-brown crystals of **1**·$2H_2O$ were collected by filtration, washed with cold acetone (2 × 7 mL) and Et_2O (2 × 7 mL), and dried in vacuo. The yield was 1.06 g (40% based on Mn). X-ray quality crystals were available from the bulk synthesis. Anal. Calcd (Found) for **1**·$2H_2O$: C, 25.13 (25.21); H, 2.59 (2.32); N, 11.99 (11.70). Selected IR data (KBr, cm^{-1}): 3400(s, br), 1602(m), 1560(w), 1498-(m), 1470(m), 1446(s), 1384(s), 1310(s), 1286(m), 1170(w), 1158-(w), 1107(w), 1073(w), 1060(w), 1035(m), 825(w), 811(w), 772(s), 738(w), 715(m), 693(w), 670(m), 655(m), 630(s), 592 (m), 419-(w).

$[CeMn_6O_9(O_2CMe)_9(NO_3)(H_2O)_2]$ (2). An orange solution of $(NH_4)_2[Ce(NO_3)_6]$ (6.78 g, 12.4 mmol) in H_2O/HO_2CMe (7/7 mL) was slowly added to an almost colorless, stirred solution of Mn-$(O_2CMe)_2{\cdot}4H_2O$ (2.02 g, 8.2 mmol) in H_2O/HO_2CMe (4/4 mL). The resultant dark reddish-brown solution was left undisturbed at room temperature. After 2 days, the black crystals of **2**·H_2O·$4HO_2$-CMe that had been formed were collected by filtration, washed with ∼10 mL each of cold acetone and Et_2O, and dried in vacuo. The yield was 0.98 g (54% based on Mn). X-ray quality crystals of the compound were available from the bulk synthesis. Anal. Calcd (Found) for **2**·H_2O·HO_2CMe: C, 18.18 (18.03); H, 2.82 (3.00); N, 1.06 (1.36). Selected IR data (KBr, cm^{-1}): 3423(s, br), 1715(w), 1627(m), 1555(s), 1495(m), 1421(s), 1384(s), 1352(m), 1046(m), 1030(m), 951(m), 839(w), 746(m), 693(m), 668(m), 628-(s), 500(m), 434(w).

$[CeMn_6O_9(O_2CMe)_9(H_2O)_2(MeOH)](ClO_4)$ (3). To a stirred colorless solution of $Mn(O_2CMe)_2{\cdot}4H_2O$ (2.02 g, 8.2 mmol) in $H_2O/MeCO_2H$ (4/4 mL) was slowly added an orange mixture of a 0.5 M solution in $HClO_4$ of $Ce(ClO_4)_4$ (24.6 mL, 12.3 mmol) and a few drops of MeOH (∼0.2 mL). The resulting dark reddish-brown solution was maintained at room temperature for approximately one week. The black crystals of **3**·$3H_2O$·0.5 $MeCO_2H$ that formed were collected by filtration, washed with ∼5 mL each of cold acetone and Et_2O, and dried in vacuo. The yield was 0.70 g (37% based on Ce). Anal. Calcd (Found) for **3**·$3H_2O$·$0.5MeCO_2H$: C 17.20 (16.90), H 3.10 (3.00). Selected IR data (KBr, cm^{-1}): 3421-(s, br), 1635(w), 1555(s), 1493(m), 1421(s), 1352(m), 1144(m), 1110(s), 1090(s), 1046(m), 1030(m), 951(w), 746(m), 693(m), 668-(m), 628(s), 500(m), 430(w).

$[Ce_3Mn_2O_6(O_2CMe)_6(NO_3)_2(mhpH)_4]$ (4). To a stirred pale yellow-brown solution of $Mn(O_2CMe)_2{\cdot}4H_2O$ (2.02 g, 8.2 mmol) and mhpH (2.00 g, 18.3 mmol) in H_2O/HO_2CMe (6/1.5 mL) was slowly added an orange solution of $(NH_4)_2[Ce(NO_3)_6]$ (6.78 g, 12.4 mmol) in H_2O/HO_2CMe (9/5 mL), resulting in a dark reddish-brown solution. This was allowed to slowly evaporate at ambient temperature, and after a few days, the now dark red solution had started to produce dark red crystals. After a few more days, the formation of the large well-shaped red crystals of **4**·$2H_2O$ was judged to be complete, and they were collected by filtration, washed with 2 × 6 mL each of acetone and Et_2O, and dried in vacuo. The yield was

(4) (a) Bhaduri, S.; Tasiopoulos, A. J.; Bolcar, M. A.; Abboud, K. A.; Streib, W. E.; Christou, G. *Inorg. Chem.* **2003**, *42*, 1483. (b) Reddy, K. R.; Rajasekharan, M. V.; Padhye, S.; Dahan, F.; Tuchagues, J.-P. *Inorg. Chem.* **1994**, *33*, 428. (c) Reddy, K. R.; Rajasekharan, M. V.; Arulsamy, N.; Hodgson, D. J. *Inorg. Chem.* **1996**, *35*, 2283. (d) Dimitrou, K.; Brown, A. D.; Concolino, T. E.; Rheingold, A. L.; Christou, G. *Chem. Commun.* **2001**, 1284.

(5) (a) *Manganese Compounds as Oxidizing Agents in Organic Chemistry*; Arndt, D., Ed.; Open Court Publishing Company: Chicago, IL, 1981. (b) Snider, B. B. *Chem. Rev.* **1996**, *96*, 339.

(6) (a) Ho, T.-L. *Organic Syntheses By Oxidation With Metal Compounds*; Mijs, W. J., de Jonge, C. R. H. I., Eds.; Plenum Press: New York, 1986; Chapter 11, pp 569−631. (b) Nair, V.; Mathew, J.; Prabhakaran, J. *Chem. Soc. Rev.* **1997**, 127.

(7) (a) Cao, H.; Suib, S. L. *J. Am. Chem. Soc.* **1994**, *116*, 5334. (b) Zaki, M. I.; Hasan, M. A.; Pasupulety, L.; Kumary, K. *New J. Chem.* **1998**, 875. (c) Trovarelli, A. *Catal. Rev.* **1996**, *38*, 439.

(8) (a) Matatov-Meytal, Y. I.; Sheintuch, M. *Ind. Eng. Chem. Res.* **1998**, *37*, 309. (b) Inamura, S.; Dol, A.; Ishida, S. *Ind. Eng. Chem. Prod. Res. Dev.* **1985**, *24*, 75. (c) Hamoudi, S.; Belkacemi, K.; Larachi, F. *Chem. Eng. Sci.* **1999**, *54*, 3569. (d) Hamoudi, S.; Belkacemi, K.; Sayari, A.; Larachi, F. *Chem. Eng. Sci.* **2001**, *56*, 1275. (e) Ding, Z. Y.; Frisch, M. A.; Li, L.; Gloyna, E. F. *Ind. Eng. Chem. Res.* **1996**, *35*, 3257. (f) Ding, Z. Y.; Li, L.; Wade, D.; Gloyna, E. F. *Ind. Eng. Chem. Res.* **1998**, *37*, 1707.

(9) (a) Tasiopoulos, A. J.; Wernsdorfer, W.; Moulton, B.; Zaworotko, M. J.; Christou, G. *J. Am. Chem. Soc.* **2003**, *125*, 15274. (b) Tasiopoulos, A. J.; O'Brien, T. A.; Abboud, K. A.; Christou, G. *Angew. Chem., Int. Ed.* **2004**, *43*, 345. (c) Murugesu, M.; Mishra, A.; Wernsdorfer, W.; Abboud, K. A.; Christou, G. *Polyhedron*, **2006**, *25*, 613−625.

Table 1. Crystallographic Data for Complexes **1**−**6**

	1	**2**	**3**	**4**	**5**	**6**
formula	$C_{22}H_{27}CeMn_2N_9O_{24}$[a]	$C_{26}H_{49}CeMn_6NO_{41}$[b]	$C_{20}H_{43}CeMn_6ClO_{38}$[c]	$C_{36}H_{50}Ce_3Mn_2N_6O_{30}$[d]	$C_{24}H_{50}Ce_3Mn_2N_4O_{35}$[e]	$C_{62}H_{93}Ce_6Mn_4N_{13}O_{69}$
fw (g/mol)	1051.53	1501.42	1396.73	1577.04	1484.92	3184.98
space group	$P\bar{1}$	$P\bar{1}$	$P\bar{1}$	*Aba*2	*C*2/c	*P*2/c
a (Å)	9.313(1)	12.562(1)	12.213(1)	22.671(2)	12.698(1)	18.482(2)
b (Å)	12.387(1)	12.915(1)	13.011(1)	14.874(1)	15. 925(1)	15.440(1)
c (Å)	17.490(2)	16.158(2)	16.634(1)	15.729(1)	23.486(2)	18.859(2)
β (deg)	83.87(1)	100.689(2)	101.581(2)	90	97.805(2)	104.376(2)
V (Å^3)	1938.8(2)	2246.8(2)	2336.5(2)	5303.6(5)	4705.0(4)	5213.3(5)
Z	2	2	2	4	4	4
T (K)	173	173	173	173	173	173
radiation	Mo Kα	Mo Kα	Mo Kα	Mo Kα	Mo Kα	Mo Kα
ρ_{calcd} (g/cm^3)	1.801	2.219	1.982	1.970	2.096	2.029
μ (mm^{-1})	1.895	2.751	2.687	3.083	3.474	3.144
R1[f,g]	8.06	4.43	7.28	2.50	2.13	5.71
wR2[f,h]	17.43	8.44	15.94	6.61	5.08	12.56

[a] **1**·2H$_2$O. [b] **2**·H$_2$O·4MeCO$_2$H. [c] **3**·3H$_2$O·1/2MeCO$_2$H. [d] **4**·2H$_2$O. [e] **5**·2H$_2$O·2MeCO$_2$H. [f] $I > 2\sigma(I)$. [g] $R1 = 100\sum(||F_o| - |F_c||)/\sum|F_o|$. [h] $wR2 = 100[\sum[w(F_o^2 - F_c^2)^2]/\sum[w(F_o^2)^2]]^{1/2}$, $w = 1/[\sigma^2(F_o^2) + [(ap)^2 + bp]$, where $p = [\max(F_o^2, 0) + 2F_c^2]/3$.

1.15 g (24% based on Ce). X-ray quality crystals were available from the bulk synthesis. Anal. Calcd (Found) for **4**·2H$_2$O: C, 27.41 (27.60); H, 3.20 (3.00); N, 5.33 (5.02). Selected IR data (KBr, cm^{-1}): 3431(s, br), 3256(m), 3100(w), 2931(m), 1635(s), 1618-(s), 1542(s),1417(s), 1384(s), 1349(m), 1292(m), 1165 (m), 1028-(m), 1004(m), 804(m), 745(m), 669 (m), 623 (s), 610(s), 578(s), 505(m), 490(m), 438(m).

[Ce$_3$Mn$_2$O$_6$(O$_2$CMe)$_6$(NO$_3$)$_2$(pyroH)$_2$(H$_2$O)$_3$] (5). To a stirred pale yellow-brown solution of Mn(O$_2$CMe)$_2$·4H$_2$O (2.02 g, 8.2 mmol) and pyroH (1.5 g, 17.6 mmol) in H$_2$O/HO$_2$CMe (5/1 mL) was slowly added an orange solution of (NH$_4$)$_2$[Ce(NO$_3$)$_6$] (6.78 g, 12.4 mmol) in H$_2$O/HO$_2$CMe (7/6 mL). After ∼10 min of stirring, the solution had become dark reddish-brown, and this was left to slowly evaporate undisturbed at ambient temperature. After 3−4 days, it was filtered to remove a brownish powder, and the filtrate was again left to slowly evaporate at room temperature. After a few more days, red crystals of **5**·2H$_2$O·2MeCO$_2$H began to form, and when their formation was judged to be complete (a few more days), they were collected by filtration, washed with 2 × 8 mL each of acetone and Et$_2$O, and dried in vacuo. The yield was 1.05 g (17% based on Ce). X-ray quality crystals were available from the bulk synthesis. Anal. Calcd (Found) for **5**·2H$_2$O·2HO$_2$CMe: C, 19.41 (19.22); H, 3.39 (3.16); N, 3.77 (3.82). Selected IR data (KBr, cm^{-1}): 3442(s, br), 2997(w), 1639(s), 1603(m), 1538(s), 1494(m), 1452(s), 1405(s), 1384(s), 1351(m), 1293(m), 1052 (w), 1032(m), 810(w), 740(w), 685(m), 669(m), 624(s), 552(w), 492-(m), 421(m).

{{(pyH)$_3$[Ce$_3$Mn$_2$O$_6$(O$_2$CMe)$_{7.5}$(NO$_3$)$_3$]·(HO$_2$CMe)$_{0.5}$·(H$_2$O)$_2$}$_2$-(NO$_3$)}$_n$ (6). To a stirred pale yellow-brown solution of Mn(O$_2$-CMe)$_2$·4H$_2$O (2.02 g, 8.2 mmol) in H$_2$O/HO$_2$CMe/pyridine (5/1/3 mL) was slowly added an orange solution of (NH$_4$)$_2$[Ce(NO$_3$)$_6$] (6.78 g, 12.4 mmol) in H$_2$O/HO$_2$CMe (7/6 mL). After ∼10 min of additional stirring, the solution had become red, and it was left to slowly evaporate at ambient temperature; dark red crystals of **6** began to form within an hour. After a few days, the formation of red crystals was judged to be complete, and they were collected by filtration, washed with 2 × 8 mL each of acetone and Et$_2$O, and dried in vacuo. The yield was 2.15 g (33% based on Ce). X-ray quality crystals were available from the bulk synthesis. Anal. Calcd (Found) for **6**: C, 23.38 (23.45); H, 2.94 (2.82); N, 5.72 (5.92). Selected IR data (KBr, cm^{-1}): 3422(s, br), 3245(m), 3179(m), 3139(m), 3111(m), 1718(w), 1635(w), 1614(m), 1540(s), 1489(s), 1417(s), 1384(s), 1349(m), 1290(m), 1201(w), 1169 (w), 1024-(m), 812(m), 755(m), 783(m), 680 (m), 621 (s), 540(w), 480(m), 505(m), 438(m).

[CeMn$_6$O$_9$(O$_2$CEt)$_9$(NO$_3$)(H$_2$O)$_2$] (7). A stirred orange solution of (NH$_4$)$_2$[Ce(NO$_3$)$_6$] (6.78 g, 12.4 mmol) in H$_2$O/HO$_2$CEt (7/7 mL) was added to an almost colorless solution of MnCl$_2$·4H$_2$O (1.64 g, 8.3 mmol) in H$_2$O/HO$_2$CEt (4/4 mL). The resultant dark reddish-brown solution was left undisturbed at room temperature; black crystals began to appear within a few hours. After 2 days, crystallization was judged to be complete, and the black crystals were collected by filtration, washed with ∼5 mL of cold acetone and Et$_2$O, and dried in vacuo. The yield was 0.60 g (42% based on Ce). Anal. Calcd (Found) for **7**·H$_2$O: C, 23.37 (23.03); H, 3.71 (3.85); N, 1.01 (1.31). Selected IR data (KBr, cm^{-1}): 3412(s, br), 2983(m), 2941(m), 1635(m), 1550(s), 1500(m), 1465(m), 1421(s), 1384(s), 1302(m), 1083(m), 1014(m), 809(w), 743(m), 628(s), 502-(m), 420(w).

X-ray Crystallography. Data for complexes **1**−**6** were collected at 173 K on a Siemens SMART PLATFORM equipped with a CCD area detector and a graphite monochromator using Mo Kα radiation (λ = 0.71073 Å). Data collection parameters are listed in Table 1. Cell parameters were refined using up to 8192 reflections. A full sphere of data (1381 frames) was collected using the ω-scan method (0.3° frame width). The first 50 frames were remeasured at the end of data collection to monitor instrument and crystal stability (maximum correction on *I* was <1%). Absorption corrections by integration were applied, based on measured indexed crystal faces. The structures were solved by direct methods in SHELXTL6[10] and refined using full-matrix least-squares. Non-hydrogen atoms were refined anisotropically, whereas hydrogen atoms were placed in ideal, calculated positions, with isotropic thermal parameters riding on their respective carbon atoms.

Complex **1**·2H$_2$O crystallizes in triclinic space group $P\bar{1}$ with the asymmetric unit containing the cation of **1**, two 50% occupancy nitrate anions, and two water molecules of crystallization. One of the nitrate anions is disordered over a center of inversion, whereas the other one is in general position. A bound nitrate is also disordered and was refined in two parts with the geometries constrained to remain equivalent. The two water molecules of crystallization are disordered, and each was refined in two parts. A total of 517 parameters were refined in the final cycle of refinement on F^2. Complex **2**·H$_2$O·4HO$_2$CMe crystallizes in triclinic space group $P\bar{1}$ with the asymmetric unit consisting of the Mn cluster, a water molecule and four acetic acid molecules of crystallization. The latter were disordered and could not be modeled properly, thus the program SQUEEZE, a part of the PLATON

(10) Sheldrick, G. M. *SHELXTL6*; Bruker-AXS, Madison, WI, 2000.

package of crystallographic software, was used to calculate the solvent disorder area and remove its contribution to the overall intensity data.[11] The nitrate group ligated to the Ce ion is severely disordered and its identification was based not only on the crystallographic data but also on spectroscopic data. A total of 530 parameters were refined in the final cycle of refinement on F^2. Compound **3**·3H_2O·0.5 $MeCO_2H$ crystallizes in triclinic space group $P\bar{1}$ with the asymmetric unit consisting of the cation of **3**, a ClO_4^- anion disordered over two positions with three waters and a half acetic acid molecules of crystallization. One of the lattice water molecules is disordered over two positions, whereas the other two water molecules are disordered against the ClO_4^- anions. A total of 642 parameters were refined in the final cycle of refinement on F^2. Compound **4**·2H_2O crystallizes in orthorhombic space group *Aba*2 with the asymmetric unit consisting of a half cluster located on a 2-fold rotation axis and a water molecule of crystallization. A total of 360 parameters were refined in the final cycle of refinement on F^2. Compound **5**·2H_2O·2$MeCO_2H$ crystallizes in monoclinic space group *C*2/*c* with the asymmetric unit consisting of a half cluster with one molecule each of water and acetic acid solvents of crystallization. A total of 350 parameters were refined in the final cycle of refinement on F^2. Compound **6** crystallizes in monoclinic space group *P*2/*c* with the asymmetric unit consisting of a Ce_3Mn_2 cluster, three pyridinium cations (one of which is disordered over two sites), two-quarter nitrate ions near centers of inversion, two water molecules disordered over three positions, and a half acetic acid disordered over a center of inversion. The Ce_3Mn_2 cluster is part of a chain structure, with each cluster joined through one acetate bridge on one side and two acetate bridges on the other. A total of 788 parameters (and 359 constraints) were refined in the final cycle of refinement on F^2.

Physical Measurements. IR spectra were recorded on KBr pellets using a Nicolet model Nexus 670 spectrophotometer. DC magnetic susceptibility data were collected on powdered, microcrystalline samples on a Quantum Design MPMS-XL SQUID magnetometer equipped with a 7 T (70kG) magnet. Diamagnetic corrections to the observed susceptibilities were applied using Pascal's constants. The exchange interactions in **3** were calculated using matrix diagonalization methods described elsewhere.[12]

Theoretical Calculations. The semiempirical molecular orbital method ZILSH[12a] was used to estimate the exchange constants for compounds **1** and **3**. According to the ZILSH procedure, energies and wavefunctions are obtained with the INDO/S method of Zerner[13] for spin components in which the spins of certain metals are reversed relative to the others. Spin couplings $\langle S_A S_B \rangle$ (A, B are metal ions) appearing in the Heisenberg spin Hamiltonian are obtained with the local spin operator method of Davidson.[14] The energies and spin couplings are assumed to follow an effective Heisenberg formula of eq 1, where *i* labels the spin component

$$E^i = E_0 - \sum_{A<B} J_{AB} \langle S_A S_B \rangle \qquad (1)$$

and E_0 contains all spin-independent contributions to the energy. Given the energies and spin couplings for the correct number of components, multiple eqs 1 can be solved simultaneously for E_0 and the exchange constants.

The calculations also provide for each metal ion the *z* component of its spin, M_i, equal to half of the number of unpaired electrons. This quantity indicates if the correct oxidation states and metal d-electron configurations were obtained for the metal ions. Finally, the calculations also provide the atomic bond index (ABI)[15] between metal and ligand atoms, with values of 1.00 reflecting a formal single bond, 2.00 a formal double bond, etc. These indices are used to rationalize the observed sign and magnitudes of the exchange constants found for compounds **1** and **3** (vide infra).

Results and Discussion

Syntheses. The compounds to be described resulted from an investigation of the oxidation of Mn^{II} reagents by Ce^{IV} under a variety of conditions. Ce^{IV} is a strong one-electron oxidant ($E° = 1.61$ V vs NHE), and it is quite capable of oxidizing Mn^{II} to Mn^{III} or Mn^{IV}. In fact, Ce^{IV} has been used previously to prepare some higher oxidation state Mn complexes. For example, oxidation of $[Mn^{II}X_2]$·4H_2O ($X = Cl^-$, F^-) in H_2O/HO_2CMe by $(NH_4)_2Ce(NO_3)_6$ in the presence of bpy gave the asymmetric dinuclear complexes $[Mn_2O_2(O_2CMe)X(H_2O)(bpy)_2]^{2+}$.[4a] Similarly, oxidation of a $H_2O/MeCO_2H/HClO_4$ solution of $[Mn(O_2CMe)_2]$·4H_2O with Ce^{IV} in the presence of bpy produced $[Mn^{IV}_2O_2(O_2CMe)(H_2O)_2(bpy)_2]^{3+}$.[4b] In contrast to such previous results, the present work has yielded mixed-metal Mn/Ce products for the first time.

Many reaction systems under a variety of conditions and reagent ratios were explored before the procedures described below were developed. These are all variations, to some degree or other, of the comproportionation reaction between Mn^{II} and Mn^{VII} that is the standard procedure for the preparation of $[Mn_{12}O_{12}(O_2CMe)_{16}(H_2O)_4]$.[3b,c] The latter involves the reaction in concentrated (60%) aqueous acetic acid between $[Mn(O_2CMe)_2]$·4H_2O and $KMnO_4$ in a Mn^{II}/Mn^{VII} ratio that gives an average of $Mn^{3.33+}$. We have modified this by substituting a Ce^{IV} source as the oxidant in place of $KMnO_4$, hoping for mixed-metal products, and also exploring reactions in which additional reagents (e.g., potentially chelating groups) were also present.

The reaction of $Mn(NO_3)_2$·*x*H_2O and bpy with $(NH_4)_2[Ce(NO_3)_6]$ in a 1:1:2 molar ratio in 25% aqueous acetic acid gave $[CeMn_2O_3(O_2CMe)(NO_3)_4(H_2O)_2(bpy)_2](NO_3)$ (**1**) in 40% isolated yield. This reaction system is very similar to those that gave the homometallic Mn^{IV}_2 products mentioned above,[4a,b] and the important factor that led to a mixed-metal product is undoubtedly the presence of the nitrate groups. There are likely several species in equilibrium in solution, and the nitrate groups favor binding to Ce^{IV} and also lead to lower solubility in organic solvents, thus favoring crystallization of nitrate-rich complex **1**. Its formation is summarized in eq 2, using the Ce/Mn reagent stoichiometry and assuming the involvement of O_2 (vide infra). Complex **1** is the lowest nuclearity product reported in this work, and this of course is consistent with the presence of bpy groups, which

(11) (a) Spek, A. L. *Acta Crystallogr., Sect. A.* **1990**, *46*, C34. (b) van der Sluis, P.; Spek, A. L. *Acta Crystallogr., Sect. A* **1990**, *46*, 194−201.
(12) (a) O'Brien, T. A.; Davidson, E. R. *Int. J. Quantum Chem.* **2003**, *92*, 294. (b) Canada-Vilalta, C.; O'Brien, T. A.; Brechin, E. K.; Pink, M.; Davidson, E. R.; Christou, G. *Inorg. Chem.* **2004**, *43*, 5505. (c) Canada-Vilalta, C.; O'Brien, T. A.; Pink, M.; Davidson, E. R.; Christou, G. *Inorg. Chem.* **2003**, *42*, 7819.
(13) Zerner, M. C.; Loew, G. H.; Kirchner, R. F.; Mueller-Westerhoff, U. T. *J. Am. Chem. Soc.* **1980**, *102*, 589.
(14) Clark, A. E.; Davidson, E. R. *J. Chem. Phys.* **2001**, *115*, 7382.
(15) Wiberg, K. B. *Tetrahedron* **1968**, *24*, 1083.

$$2Mn^{2+} + 4Ce^{4+} + 4NO_3^- + 2bpy + MeCO_2H + 5H_2O + {}^1/_4O_2 \rightarrow 3Ce^{3+} + 6H^+ + {}^1/_2H_2O + [CeMn_2O_3(O_2CMe)(NO_3)_4(H_2O)_2(bpy)_2]^+ \quad (2)$$

are effective chelates but not bridging groups and thus discourage formation of high nuclearity species.

The reaction of $Mn(O_2CMe)_2 \cdot 4H_2O$ and $(NH_4)_2[Ce(NO_3)_6]$ in a 2:3 molar ratio in concentrated (50%) aqueous acetic acid gave $[CeMn_6O_9(O_2CMe)_9(NO_3)(H_2O)_2]$ (**2**) in 54% isolated yield. The formation of this much higher nuclearity product is summarized in eq 3

$$6Mn(O_2CMe)_2 + 9Ce^{4+} + NO_3^- + 11H_2O + O_2 \rightarrow [CeMn_6O_9(O_2CMe)_9(NO_3)(H_2O)_2] + 8Ce^{3+} + 3MeCO_2^- + 14H^+ + 2H_2O \quad (3)$$

When this reaction was repeated but with a 0.5 M solution of $Ce(ClO_4)_4$ in aqueous $HClO_4$ as the oxidizing agent, plus a few drops of MeOH, the product was now the structurally related complex $[CeMn_6O_9(O_2CMe)_9(H_2O)_2(MeOH)](ClO_4)$ (**3**) in 37% yield. We initially obtained this compound in low yield from a reaction without MeOH and were surprised to see the MeOH ligand, which must have formed in situ; subsequent addition of a few drops of MeOH to the reaction mixture gave much increased yields. The isolation of the MeOH-containing complex **3** is presumably the result of relative solubilities compared with other possible forms, such as that with a third H_2O terminal ligand. The analogous reaction using propionic acid instead of acetic acid and $(NH_4)_2[Ce(NO_3)_6]$ as the oxidizing agent gave $[CeMn_6O_9(O_2CEt)_9(NO_3)(H_2O)_2] \cdot H_2O$ (**7**), identified by elemental analysis and spectroscopic comparison with **2**. Its alternative formulation as $[Mn_6CeO_9(O_2CEt)_9(H_2O)_3](NO_3)$, analogous to **3** but with an extra H_2O in place of the MeOH, cannot be ruled out but is less favored given the better ligating properties of nitrate versus those of perchlorate.

Further Ce/Mn products were obtained from reactions performed in the presence of 2-hydroxy-6-methylpyridine (mhpH) with a less-concentrated solution of aqueous acetic acid. The addition of potentially chelating mhpH was based on the observation that it had been successfully employed by others for the synthesis of a number of metal complexes, including several mixed 3d−4f metal clusters.[16] We found that the reaction of $Mn(O_2CMe)_2 \cdot 4H_2O$, $(NH_4)_2[Ce(NO_3)_6]$, and mhpH in a 2:3:∼4.4 ratio in 30% aqueous acetic acid gave $[Ce_3Mn_2O_6(O_2CMe)_6(NO_3)_2(mhpH)_4]$ (**4**) in 24% yield (eq 4). We found it interesting that the mhpH stayed

$$2Mn^{2+} + 3Ce^{4+} + 4mhpH + 6MeCO_2H + 4H_2O + 2NO_3^- + O_2 \rightarrow 14H^+ + [Ce_3Mn_2O_6(O_2CMe)_6(NO_3)_2(mhpH)_4] \quad (4)$$

protonated and bound in a monodentate fashion (vide infra), and the reaction was thus repeated instead with a similar organic molecule, 2-pyrrolidinone (pyroH), which has also been successfully employed in the past for the synthesis of mixed-metal 3d−4f complexes;[17] a clean product was obtained using a slightly more concentrated (37%) aqueous acetic acid solution, and it was identified as $[Ce_3Mn_2O_6(O_2CMe)_6(NO_3)_2(pyroH)_2(H_2O)_3]$ (**5**), obtained in a 17% yield (eq 5). The structure of **5** is very similar to that of **4**,

$$2Mn^{2+} + 3Ce^{4+} + 2pyroH + 6MeCO_2H + 6H_2O + 2NO_3^- + O_2 \rightarrow 14H^+ + [Ce_3Mn_2O_6(O_2CMe)_6(NO_3)_2(pyroH)_2(H_2O)_2] \quad (5)$$

containing protonated, monodentate pyroH groups (vide infra). Finally, the procedure was repeated but with an excess of pyridine instead of mhpH or pyroH, and the same Ce_3Mn_2 core was obtained, but this time within the polymer $\{\{(pyrH)_3[Ce_3Mn_2O_6(O_2CMe)_{7.5}(NO_3)_3] \cdot (HO_2CMe)_{0.5} \cdot (H_2O)_2\}_2(NO_3)\}_n$ (**6**), isolated in 33% yield.

Complexes **1**−**7** span a wide range of Ce/Mn ratios, from Ce_3Mn_2 in **4**−**6**, $CeMn_2$ in **1**, to $CeMn_6$ in **2**, **3** and **7**. Other combinations are no doubt also possible as this work is extended. It is also particularly noteworthy that although the Ce/Mn ratios change so much, something else is constant for all seven described complexes, and that is the metal oxidation levels: in all complexes, both the Ce and Mn atoms are in the +4 oxidation state. This is even more interesting when it is remembered that in all the described reactions Ce^{IV} was used as the oxidant of Mn^{II}, and the Ce^{IV}/Mn^{II} reaction ratios were such that all Ce^{IV} was ostensibly reduced to Ce^{III} in the generation of Mn^{IV}. Oxidation of Mn^{II} to Mn^{IV} by atmospheric O_2 is not expected under normal conditions, and the observation of only Ce^{IV}/Mn^{IV} products from the present work therefore demands some comment. We do not believe this is just happenstance, and rationalize it as follows: the oxidation by Ce^{IV} of Mn^{II} generates Mn^{III} and then Mn^{IV}. The latter is a hard acid and favors formation of non-mononuclear products containing hard O^{2-} bridging ions, the latter originating from H_2O molecules; indeed, the chemistry of Mn^{IV} is replete with such oligonuclear species.[1c,4] The presence of the hard O^{2-} ions will also in turn favor incorporation of hard Ce^{4+} ions, facilitating formation of Ce^{IV}/Mn^{IV} products, presumably involving the participation of atmospheric oxygen as the oxidant of any intermediate Ce^{III}/Mn^{IV} species formed on oxidation of Mn^{II} by Ce^{IV}. For this reason, O_2 was used to balance eqs 2−5.

Description of Structures. Crystallographic data collection and structure refinement details for compounds **1**−**6** are summarized in Table 1, and selected interatomic distances are listed in Tables 2−7. Bond valence sum (BVS) calculations (Tables 8 and 9), charge considerations, and inspection of metric parameters confirm that both Mn and Ce atoms of all the complexes are in oxidation state +4.[18]

(16) (a) Blake, A. J.; Gould, R. O.; Grant, C. M.; Milne, P. E. Y.; Parsons, S.; Winpenny, R. E. P. *J. Chem. Soc., Dalton Trans.* **1997**, 485. (b) Winpenny, R. E. P. *Chem. Soc. Rev.* **1998**, *27*, 447.

(17) Sun, X. −R.; Chen, Z. −D.; Yan, F.; Gao, S.; Cheung, K. −K.; Che, C. M.; Zhang, X. −X. *J. Cluster Sci.* **2002**, *13*, 103.

(18) (a) Liu, W.; Thorp, H. H. *Inorg. Chem.* **1993**, *32*, 4102. (b) Roulhac, P. L.; Palenik, G. J. *Inorg. Chem.* **2003**, *42*, 118.

Table 2. Selected Interatomic Distances (Å) for **1**·2H_2O

Ce−O(5)	1.945(7)	Mn(1)−O(1)	1.848(6)
Ce−O(18)	2.445(8)	Mn(1)−O(5)	1.851(7)
Ce−O(7)	2.49(3)	Mn(1)−O(4)	1.941(7)
Ce−O(15)	2.506(8)	Mn(1)−N(2)	1.992(8)
Ce−O(10)	2.518(8)	Mn(1)−N(1)	2.047(8)
Ce−O(12)	2.525(8)	Mn(1)···Mn(2)	2.659(2)
Ce−O(9)	2.539(8)	Mn(2)−O(1)	1.778(7)
Ce−O(13)	2.562(7)	Mn(2)−O(2)	1.803(7)
Ce−O(6)	2.59(3)	Mn(2)−O(3)	1.937(7)
Ce−O(16)	2.600(7)	Mn(2)−O(19)	1.987(7)
Ce···Mn(1)	3.793(2)	Mn(2)−N(3)	1.990(8)
Mn(1)−O(2)	1.806(7)	Mn(2)−N(4)	2.062(8)

Table 3. Selected Interatomic Distances (Å) for **2**·H_2O·4$MeCO_2H$

Ce−O(7)	2.283(4)	Mn(3)−O(3)	1.859(4)
Ce−O(1)	2.286(4)	Mn(3)−O(17)	1.927(4)
Ce−O(4)	2.293(4)	Mn(3)−O(16)	1.956(4)
Ce−O(28)	2.366(5)	Mn(3)−O(18)	1.963(4)
Ce−O(29)	2.408(4)	Mn(4)−O(5)	1.813(4)
Ce−O(30)	2.410(4)	Mn(4)−O(4)	1.837(4)
Ce−O(3)	2.469(4)	Mn(4)−O(6)	1.856(4)
Ce−O(6)	2.471(3)	Mn(4)−O(21)	1.962(4)
Ce−O(9)	2.472(4)	Mn(4)−O(19)	1.968(4)
Mn(1)−O(8)	1.806(4)	Mn(4)−O(20)	1.969(4)
Mn(1)−O(1)	1.838(4)	Mn(5)−O(5)	1.824(4)
Mn(1)−O(9)	1.861(4)	Mn(5)−O(7)	1.834(4)
Mn(1)−O(11)	1.930(4)	Mn(5)−O(6)	1.862(4)
Mn(1)−O(10)	1.963(4)	Mn(5)−O(24)	1.954(4)
Mn(1)−O(12)	1.978(4)	Mn(5)−O(23)	1.960(4)
Mn(2)−O(2)	1.805(4)	Mn(5)−O(22)	1.970(4)
Mn(2)−O(1)	1.825(4)	Mn(6)−O(8)	1.814(4)
Mn(2)−O(3)	1.868(4)	Mn(6)−O(7)	1.836(4)
Mn(2)−O(15)	1.949(4)	Mn(6)−O(9)	1.856(4)
Mn(2)−O(14)	1.963(4)	Mn(6)−O(26)	1.933(4)
Mn(2)−O(13)	1.978(4)	Mn(6)−O(27)	1.947(4)
Mn(3)−O(4)	1.818(4)	Mn(6)−O(25)	1.967(4)
Mn(3)−O(2)	1.819(4)		

Table 4. Selected Interatomic Distances (Å) for **3**·3H_2O·0.5$MeCO_2H$

Ce−O(6)	2.271(6)	Mn(3)−O(6)	1.830(6)
Ce−O(12)	2.274(6)	Mn(3)−O(7)	1.862(6)
Ce−O(9)	2.287(6)	Mn(3)−O(20)	1.952(7)
Ce−O(3)	2.415(7)	Mn(3)−O(19)	1.952(7)
Ce−O(2)	2.421(7)	Mn(3)−O(21)	1.962(6)
Ce−O(1)	2.440(7)	Mn(3)−Mn(4)	2.722(2)
Ce−O(4)	2.467(6)	Mn(4)−O(8)	1.817(7)
Ce−O(7)	2.479(6)	Mn(4)−O(9)	1.830(6)
Ce−O(10)	2.483(6)	Mn(4)−O(7)	1.858(6)
Ce···Mn(2)	3.362(2)	Mn(4)−O(22)	1.947(6)
Ce···Mn(5)	3.366(2)	Mn(4)−O(23)	1.956(7)
Ce···Mn(1)	3.370(2)	Mn(4)−O(24)	1.959(7)
Mn(1)−O(5)	1.794(6)	Mn(5)−O(11)	1.815(7)
Mn(1)−O(12)	1.833(6)	Mn(5)−O(9)	1.828(6)
Mn(1)−O(4)	1.863(6)	Mn(5)−O(10)	1.851(6)
Mn(1)−O(15)	1.946(7)	Mn(5)−O(26)	1.931(7)
Mn(1)−O(13)	1.949(6)	Mn(5)−O(25)	1.946(7)
Mn(1)−O(14)	1.975(6)	Mn(5)−O(27)	1.951(6)
Mn(1)···Mn(2)	2.706(2)	Mn(5)−Mn(6)	2.713(2)
Mn(2)−O(5)	1.804(6)	Mn(6)−O(11)	1.816(6)
Mn(2)−O(6)	1.835(6)	Mn(6)−O(12)	1.827(6)
Mn(2)−O(4)	1.859(6)	Mn(6)−O(10)	1.859(7)
Mn(2)−O(16)	1.942(6)	Mn(6)−O(28)	1.946(6)
Mn(2)−O(18)	1.948(7)	Mn(6)−O(29)	1.954(7)
Mn(2)−O(17)	1.960(7)	Mn(6)−O(30)	1.965(7)
Mn(3)−O(8)	1.830(6)		

A labeled ORTEP representation of the cation of **1** is shown in Figure 1. Its structure comprises a $[Mn^{IV}_2(\mu\text{-}O)_2(\mu\text{-}O_2CMe)]^{3+}$ unit linked to a Ce^{IV} atom via a linear oxide bridge. The Mn−Mn−Ce angle is 139.6(2)°. The ten-coordinate Ce^{IV} ion is additionally ligated by four chelating nitrate groups and a water molecule (O18). Near-octahedral

Table 5. Selected Interatomic Distances (Å) for **4**·2H_2O

Ce(1)−O(9′)	2.286(2)	Ce(2)−O(14′)	2.325(3)
Ce(1)−O(2)	2.308(2)	Ce(2)−O(9)	2.383(2)
Ce(1)−O(1)	2.320(2)	Ce(2)−O(9′)	2.383(2)
Ce(1)−O(4)	2.335(3)	Ce(2)−O(13)	2.386(3)
Ce(1)−O(1′)	2.383(2)	Ce(2)−O(13′)	2.386(3)
Ce(1)−O(3)	2.389(2)	Ce(2)···Mn(1′)	3.2407(6)
Ce(1)−O(5)	2.437(3)	Ce(2)···Ce(1′)	3.7316(4)
Ce1 O(7)	2.514(3)	Mn(1)−O(2)	1.826(2)
Ce(1)−O(6)	2.596(3)	Mn(1)−O(1)	1.833(3)
Ce(1)···Mn(1′)	3.2482(6)	Mn(1)−O(9)	1.836(3)
Ce(1)···Ce(2)	3.7316(4)	Mn(1)−O(11)	1.967(2)
Ce(1)···Ce(1′)	3.8107(4)	Mn(1)−O(12)	1.970(3)
Ce(2)−O(2′)	2.269(3)	Mn(1)−O(10)	1.973(3)
Ce(2)−O(2)	2.269(3)	Mn(1)···Ce(1′)	3.2482(6)
Ce(2)−O(14)	2.325(3)		

Table 6. Selected Interatomic Distances (Å) for **5**·2H_2O·2$MeCO_2H$

Ce(1)−O(4′)	2.288(2)	Ce(2)−O(11)	2.375(2)
Ce(1)−O(4)	2.296(2)	Ce(2)−O(11′)	2.375(2)
Ce(1)−O(9′)	2.310(2)	Ce(2)−O(13)	2.517(2)
Ce(1)−O(5)	2.343(2)	Ce(2)−O(13′)	2.517(2)
Ce(1)−O(3)	2.356(2)	Ce(2)−O(12)	2.529(3)
Ce(1)−O(14′)	2.425(2)	Ce(2)···Mn(1′)	3.2203(4)
Ce(1)−O(6)	2.439(2)	Ce(2)···Mn(1)	3.2203(4)
Ce(1)−O(1)	2.504(2)	Ce(2)···Ce(1′)	3.7449(3)
Ce(1)−O(2)	2.601(2)	Mn(1)−O(9)	1.821(2)
Ce(1)−N(1)	2.967(3)	Mn(1)−O(4)	1.822(2)
Ce(1)···Mn(1′)	3.2031(4)	Mn(1)−O(5)	1.829(2)
Ce(1)···Mn(1)	3.2374(4)	Mn(1)−O(7)	1.989(2)
Ce(2)−O(5′)	2.286(2)	Mn(1)−O(8)	1.994(2)
Ce(2)−O(5)	2.286(2)	Mn(1)−O(10)	2.000(2)
Ce(2)−O(9)	2.344(2)	Mn(1)···Ce(1′)	3.2031(4)
Ce(2)−O(9′)	2.344(2)		

Table 7. Selected Interatomic Distances (Å) for **6**

Ce(1)−O(4)	2.286(5)	Ce(3)−O(6)	2.311(5)
Ce(1)−O(3)	2.309(5)	Ce(3)−O(5)	2.313(5)
Ce(1)−O(1)	2.314(5)	Ce(3)−O(3)	2.323(5)
Ce(1)−O(2)	2.324(5)	Ce(3)−O(2)	2.325(5)
Ce(1)−O(10)	2.412(6)	Ce(3)−O(19)	2.334(5)
Ce(1)−O(8)	2.420(5)	Ce(3)−O(17)	2.437(6)
Ce(1)−O(9)	2.436(5)	Ce(3)−O(21)	2.444(6)
Ce(1)−O(7)	2.502(6)	Ce(3)−O(18)	2.496(5)
Ce(1)−O(11)	2.636(6)	Ce(3)−O(20)	2.636(5)
Ce(1)−N(1)	2.991(8)	Ce(3)−N(3)	3.012(7)
Ce(1)···Mn(2)	3.202(2)	Ce(3)···Mn(2)	3.223(2)
Ce(1)···Mn(1)	3.232(2)	Ce(3)···Mn(1)	3.228(2)
Ce(2)−O(6)	2.310(5)	Mn(1)−O(5)	1.826(5)
Ce(2)−O(5)	2.315(5)	Mn(1)−O(2)	1.832(5)
Ce(2)−O(1)	2.320(5)	Mn(1)−O(1)	1.834(5)
Ce(2)−O(4)	2.336(5)	Mn(1)−O(24)	1.965(5)
Ce(2)−O(15)	2.346(5)	Mn(1)−O(22)	1.972(5)
Ce(2)−O(14)	2.432(6)	Mn(1)−O(23)	1.982(5)
Ce(2)−O(12)	2.432(6)	Mn(2)−O(6)	1.819(5)
Ce(2)−O(13)	2.478(5)	Mn(2)−O(3)	1.823(5)
Ce(2)−O(16)	2.610(5)	Mn(2)−O(4)	1.837(5)
Ce(2)−N(2)	2.966(6)	Mn(2)−O(25)	1.975(5)
Ce(2)···Mn(1)	3.220(2)	Mn(2)−O(26)	1.976(6)
Ce(2)···Mn(2)	3.229(2)	Mn(2)−O(27)	1.989(6)

coordination at each Mn is completed by a chelating bpy group and a terminal water molecule (O19) at Mn2. The Mn−O and Mn−N bond lengths and the Mn···Mn separation (2.659 Å) are typical of those in discrete dinuclear complexes containing the $[Mn^{IV}_2(\mu\text{-}O)_2(\mu\text{-}O_2CMe)]^{3+}$ core.[4a] Because of the bridging acetate group, the $[Mn_2O_2]$ rhomb is not planar, as is also the case for other complexes containing this triply bridged core.[4a,b] There is a trans influence evident in the Mn1−O1 and Mn1−O5 bonds (1.848(6) and 1.851-(7) Å, respectively), which are longer than Mn1−O2 (1.806-(7) Å), Mn2−O1 (1.778(7) Å), and Mn2−O2 (1.803(7) Å),

Table 8. Bond Valence Sums for the Mn Atoms in **1**−**6**[a]

	1			2			3		
atom	Mn^{II}	Mn^{III}	Mn^{IV}	Mn^{II}	Mn^{III}	Mn^{IV}	Mn^{II}	Mn^{III}	Mn^{IV}
Mn(1)	4.37	4.07	4.16	4.28	3.91	4.10	4.31	3.94	4.14
Mn(2)	4.29	3.99	4.08	4.26	3.90	4.22	4.32	3.95	4.28
Mn(3)				4.33	3.96	4.16	4.24	3.88	4.07
Mn(4)				4.22	3.86	4.06	4.29	3.92	4.12
Mn(5)				4.22	3.86	4.05	4.37	3.99	4.19
Mn(6)				4.30	3.94	4.14	4.29	3.92	4.12

	4			5			6		
atom	Mn^{II}	Mn^{III}	Mn^{IV}	Mn^{II}	Mn^{III}	Mn^{IV}	Mn^{II}	Mn^{III}	Mn^{IV}
Mn(1)	4.23	3.87	4.06	4.17	3.82	4.01	4.22	3.86	4.05
Mn(2)							4.22	3.86	4.05

[a] The underlined value is the one closest to the charge for which it was calculated. The oxidation state of a particular atom can be taken as the nearest whole number to the underlined value.

Table 9. Bond Valence Sums for the Ce Atoms in **1**−**6**[a]

	1		2		3	
atom	Ce^{III}	Ce^{IV}	Ce^{III}	Ce^{IV}	Ce^{III}	Ce^{IV}
Ce(1)	4.61	3.99	4.51	3.91	4.43	3.84

	4		5		6	
atom	Ce^{III}	Ce^{IV}	Ce^{III}	Ce^{IV}	Ce^{III}	Ce^{IV}
Ce(1)	4.41	3.82	4.43	3.84	4.35	3.77
Ce(2)	4.46	3.86	4.40	3.81	4.39	3.80
Ce(3)					4.37	3.78

[a] See footnote of Table 8.

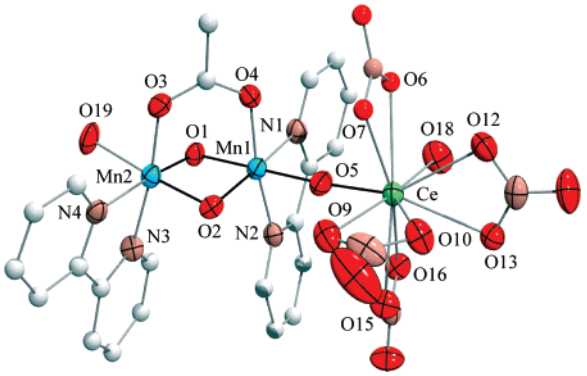

Figure 1. Labeled ORTEP plot (at the 50% probability level) of the cation of **1**. Color scheme: Mn (blue), Ce (green), O (red), N (brown), C (gray).

but otherwise Mn1−O1 and Mn1−O5 appear to be normal Mn^{IV}−O^{2-} bonds. The Ce−O bond lengths (2.44−2.60 Å) are slightly longer than is typical for ten-coordinate Ce^{IV} (Ce−O bond lengths ∼2.3−2.5 Å),[18b] probably as a consequence of the very short Ce^{IV}−O^{2-} bond (Ce−O5 = 1.945 Å), to our knowledge the shortest Ce−O bond length reported to date. Complex **1**·2H_2O is the first example of a mixed-metal Tr/Ln compound (where Tr = transition metal, Ln = lanthanide) to contain this unusual [Tr(μ-O)$_2$Tr(μ-O)-Ln] unit. A close examination of the unit cell revealed the presence of inter- and intramolecular hydrogen-bonding interactions involving the bound, as well as lattice, water and nitrate molecules.

A labeled ORTEP representation and a stereoplot of compound **2** are shown in Figure 2. The structure consists of an unprecedented Mn^{IV}_6 wheel, with the edges

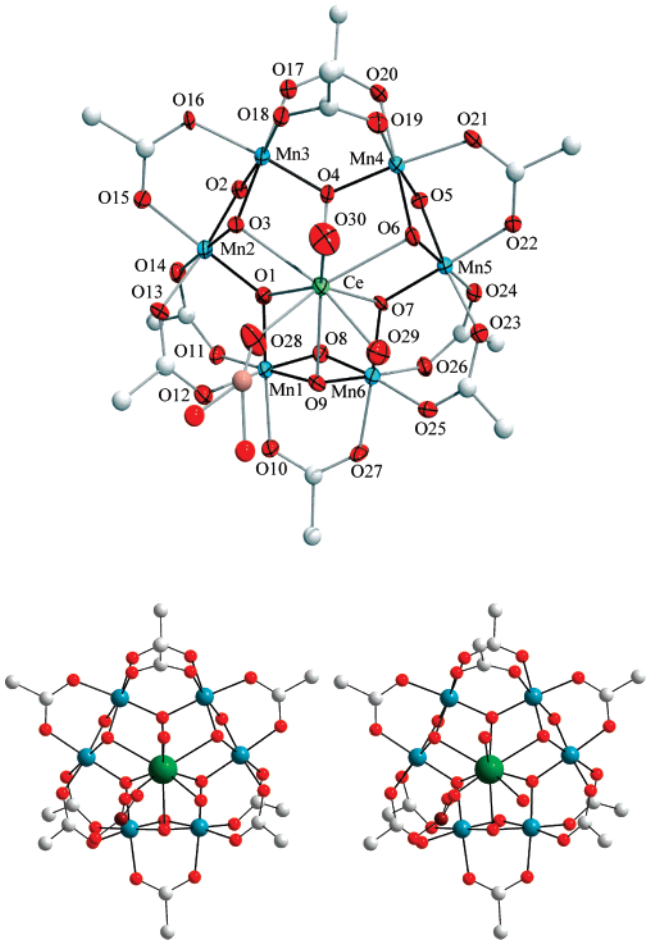

Figure 2. (a) Labeled ORTEP plot (at the 50% probability level) and (b) stereopair of **2**. Color scheme: Mn (blue), Ce (green), O (red), N (brown), C (gray).

bridged alternately by (μ-O)(μ_3-O)(μ-O_2CMe) and (μ_3-O)(μ-O_2CMe)$_2$ ligand sets giving Mn···Mn separations of 2.705 and 3.287 Å, respectively. The six μ_3-O^{2-} ions are those bound to and thus holding in place the central Ce^{IV} ion, which lies 1.513 Å above the Mn_6 ring plane and is also coordinated to two water molecules and one severely disordered monodentate nitrate group. The latter was assigned as nitrate rather than acetate based on a combination of the crystallographic data, the IR spectrum (strong sharp band at 1384 cm^{-1}), and the elemental analysis (1.36% N). The Ce−O bond lengths (2.283−2.472 Å) are within the expected range for ennea-coordinate Ce^{IV}.[18b] The Mn^{IV}−O^{2-} (1.805−1.868 Å) and Mn−O (acetate) bond lengths (1.927−1.978 Å) are typical of Mn^{IV} values. There are also intermolecular hydrogen bonds between bound H_2O groups and NO_3^- groups on neighboring molecules; there are likely additional ones involving the disordered solvent molecules of crystallization. Apart from being the first Mn^{IV}_6 wheel, complex **2** is also the first wholly Mn^{IV} complex with only oxide and carboxylate ligands, and its [M_7O_9] core (Figure 3) is of a structural type never seen before for any metal. In addition, it is one of only a few examples of a cyclic TM_6Ln complex, that is, a wheel of transition metal ions with a central lanthanide

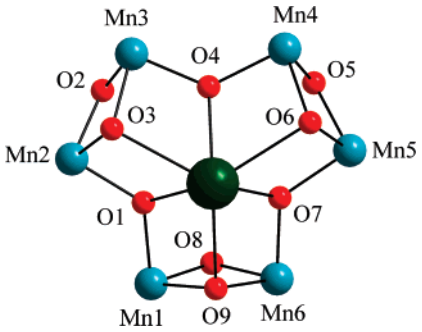

Figure 3. PovRay representation of the core of **2**. Color scheme: Mn (blue), Ce (green), O (red).

ion.[19] It is also worth noting that **2** can be considered as three $[Mn^{IV}_2(\mu\text{-}O)_2(\mu\text{-}O_2CMe)]^{3+}$ units, as present in **1**, held together by the central Ce^{IV} ion and additional acetate and oxide bridges between the dinuclear units. We recently also reported a serpentinelike Mn_8 cluster that is a linkage of $[Mn_2O_2]$ units.[3a]

Selected interatomic distances for **3** are listed in Table 4. Its structure is very similar to that of **2** with the main difference being that instead of the monodentate nitrate ligand the central Ce ion is ligated to a MeOH group. The compound is thus monocationic, and there is a ClO_4^- counterion. The structure of **3** is not discussed further here, but labeled representations of the molecule and its core are provided in the Supporting Information.

A labeled ORTEP representation and a stereoplot of complex **4** are shown in Figure 4. The molecule has crystallographically imposed C_2 symmetry with the C_2 axis passing through Ce2 and bisecting the O1···O1′ vector. The core consists of a Ce^{IV}_3 isosceles triangle, with Ce1···Ce1′ (3.8107(4) Å) slightly longer than Ce1···Ce2 and its symmetry partner (3.7316(4) Å). Each edge of the Ce_3 triangle is bridged by two μ_3-O^{2-} ions that also bridge to the two Mn^{IV} ions lying, one each above and below the Ce^{IV}_3 plane forming an M_5 trigonal bipyramid (Figure 5). The resulting Mn···Mn separation is very long at 4.818 Å. Peripheral ligation is completed by bridging acetate, chelating nitrate, and terminal mhpH groups; the latter protonated at their N atoms and binding only through their O atoms (O4 and O14). The Ce−O bond lengths are within the expected range for eight- and nine-coordinate Ce^{IV}.[18b] The Ce_3Mn_2 trigonal bipyramidal topology has been observed in mixed 4f/3d chemistry only once before, in a $Nd^{III}_3Cr^{III}_2$ complex that contains hydroxide bridges, rather than oxide ones as in **4**.[20a] In fact, there are a number of mixed 4f/3d clusters where the transition metal is linked to the lanthanide(III) ion through

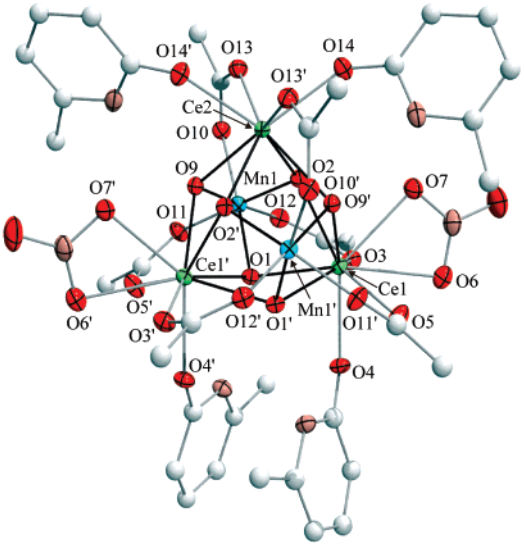

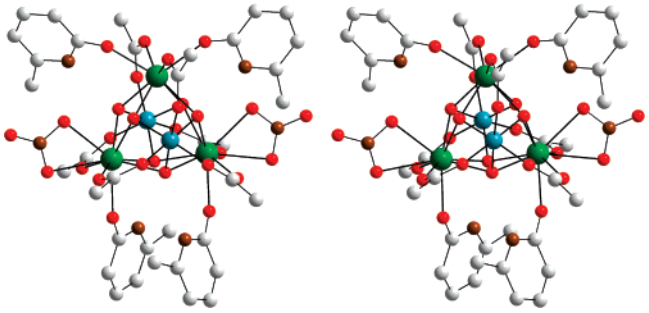

Figure 4. (a) Labeled ORTEP plot (at the 50% probability level) and (b) stereopair of **4**. Color scheme: Mn (blue), Ce (green), O (red), N (brown), C (gray).

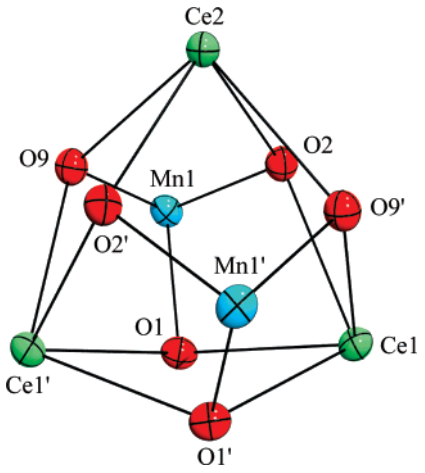

Figure 5. ORTEP representation (at the 50% probability level) of the core of **4**. Color scheme: Mn (blue), Ce (green), O (red).

μ_3-hydroxo and/or bridging carboxylate ligands,[16, 20a−d] but only a few containing μ_3-O^{2-} ions.[20e, f]

A labeled ORTEP representation of compound **5** is shown in Figure 6. Compound **5** is very similar to **4** in that it contains the same $[Ce_3Mn_2(\mu_3\text{-}O)_6]^{8+}$ core. The main differences between the two compounds are (i) the pyroH vs mhpH terminal ligands and (ii) all three Ce ions in **5** are nine-coordinate, whereas only two of those in **4** are nine-coordinate, the other being eight-coordinate.

(19) Zhang, Y.-J.; Ma, B.-Q.; Gao, S.; Li, J.-R.; Liu, Q.-D.; Wen, G.-H.; Zhang, X.-X. *Dalton Trans.* **2000**, 2249.

(20) (a) Sakagami, N.; Tsunekawa, M.; Konno, T.; Okamoto, K. *Chem. Lett.* **1997**, 575. (b) Chen, X.-M.; Aubin, S. M. J.; Wu, Y.-L.; Yang, Y.-S.; Mak, T. C. W.; Hendrickson, D. N. *J. Am. Chem. Soc.* **1995**, *117*, 9600. (c) Yang, Y.-Y.; Wu, Y.-L.; Long, L.-S.; Chen, X.-M. *J. Chem. Soc., Dalton Trans.* **1999**, 2005. (d) Yang, Y.-Y.; Chen, X.-M.; Ng, S. W. *J. Solid State Chem.* **2001**, *161*, 214. (e) Benelli, C.; Murrie, M.; Parsons, S.; Winpenny, R. E. P. *J. Chem. Soc., Dalton Trans.* **1999**, 4125. (f) Hubert-Pfalzgraf, L. G.; Abada, V.; Vaissermann, J. *Polyhedron* **1999**, *18*, 3497.

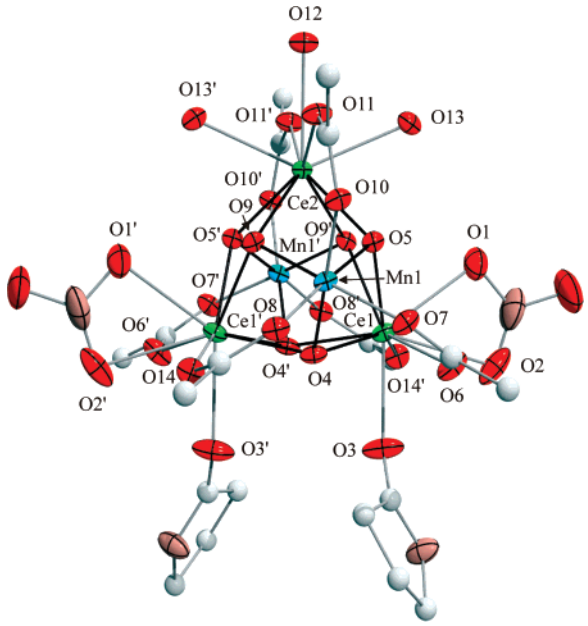

Figure 6. Labeled ORTEP plot (at the 50% probability level) of **5**. Color scheme: Mn (blue), Ce (green), O (red), N (brown), C (gray).

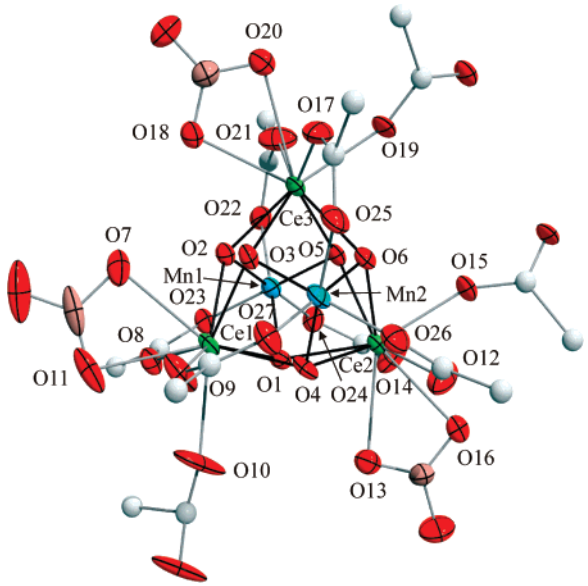

Figure 7. Labeled ORTEP plot (at the 50% probability level) of the repeating unit of the polymeric chain of **6**. Color scheme: Mn (blue), Ce (green), O (red), N (brown), C (gray).

A labeled ORTEP representation of the repeating unit of polymeric compound **6** is shown in Figure 7. It contains a $[Ce_3Mn_2(\mu_3\text{-}O)_6]^{8+}$ trigonal bipyramidal repeating unit similar to those in **4** and **5**. There are again three acetate groups on each side of the molecule, bridging each Mn atom to each of the Ce atoms. In contrast to **4** and **5**, there is now a chelating nitrate group on each Ce atom. The remaining ligand at each Ce is an acetate group that bridges to an adjacent molecule to form a one-dimensional zigzag chain structure with the molecules linked alternately by one and two acetate bridges, as shown in Figure 8. The structure can be alternatively described as a dimer of $[Ce_3Mn_2(\mu_3\text{-}O)_6]^{8+}$ units linked by two acetate bridging ligands, which is connected to the other dimer units by an acetate group to form a polymer of dimers. The chains all run parallel in the crystal, as is emphasized in Figure 9 which shows a section of some polymeric chains.

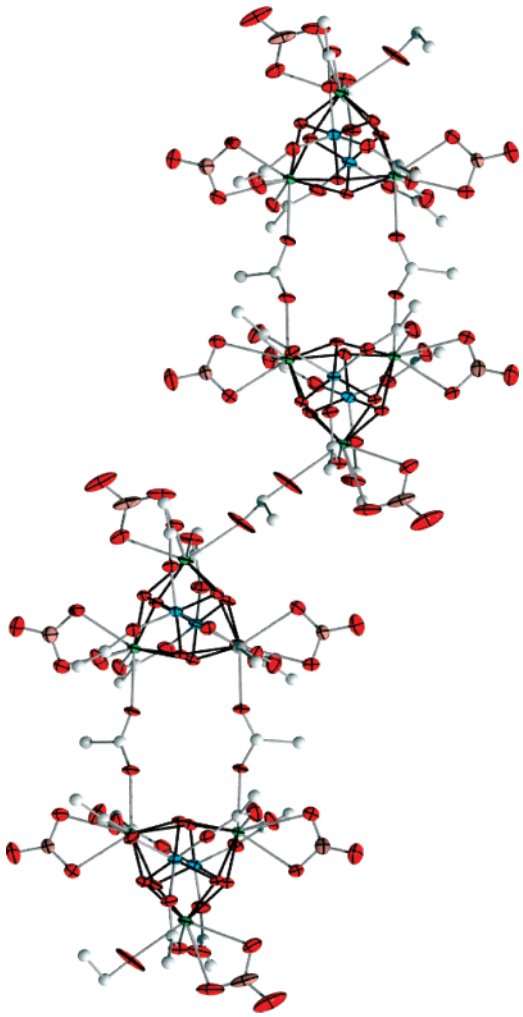

Figure 8. ORTEP representation (at the 50% probability level) of a section of the chain of **6**. Color scheme: Mn (blue), Ce (green), O (red), N (brown), C (gray).

Magnetic Susceptibility Studies. Solid-state magnetic susceptibility (χ_M) measurements were carried out on vacuum-dried, microcrystalline samples of complexes **1**−**6** in the temperature range of 5.0−300 K in a 0.5 T field.

$\chi_M T$ for $CeMn_2$ complex **1** decreases rapidly from 1.94 $cm^3\ mol^{-1}\ K$ at 300 K to 0.23 $cm^3\ mol^{-1}\ K$ at 40.0 K and then to 0.06 $cm^3\ mol^{-1}\ K$ at 5.0 K (Figure 10). The 300 K value is much smaller than the expected 3.75 $cm^3\ mol^{-1}\ K$ for two non-interacting Mn^{IV} centers, indicating the presence of strong antiferromagnetic interactions. This is supported by the steady decrease in $\chi_M T$ with decreasing temperature, reaching a near diamagnetic value at 5.0 K. We conclude there is an antiferromagnetic exchange interaction between the Mn^{IV} centers, and a resulting $S_T = 0$ molecular ground state. This conclusion is supported by the theoretical calculations described below. $\chi_M T$ for Ce_3Mn_2 complex **4** decreases only slightly from 3.92 $cm^3\ mol^{-1}\ K$ at 300 K to 3.76 $cm^3\ mol^{-1}\ K$ at 100 K and then more rapidly to 2.60 $cm^3\ mol^{-1}\ K$ at 5.0 K (Figure 11). The room-temperature $\chi_M T$ value is essentially that expected for two non-interacting Mn^{IV}

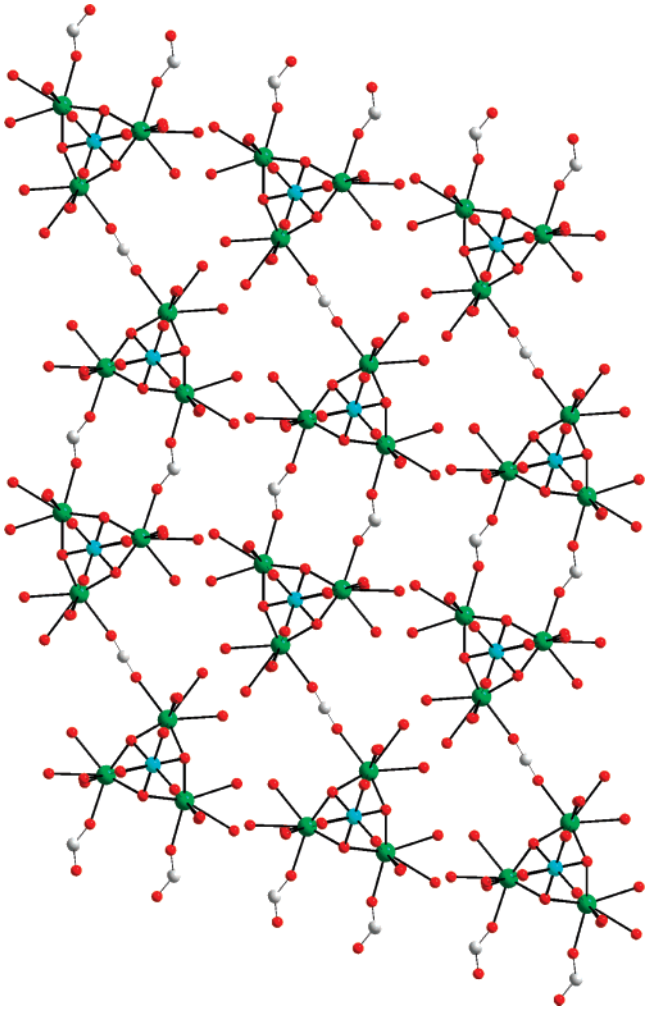

Figure 9. Section of three adjacent chains of **6** emphasizing their parallel registry. Only atoms bound to the metal atoms are shown, except for the C atoms in the bridging carboxylate groups. Color scheme: Mn (blue), Ce (green), O (red), C (gray).

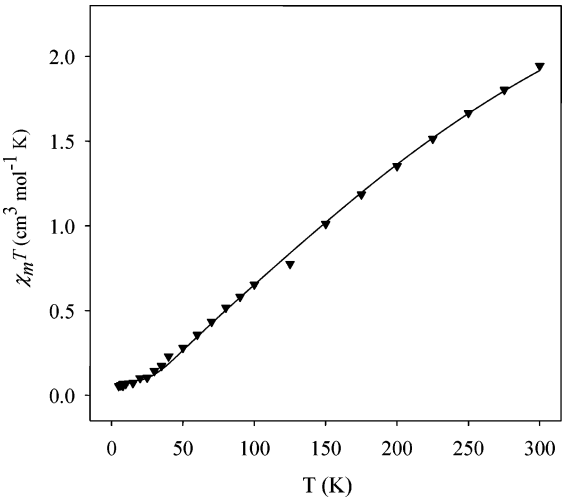

Figure 10. Plot of $\chi_M T$ vs T for complex **1**. The solid line is the fit of the data; see the text for the fit parameters.

centers, and the decreasing $\chi_M T$ with decreasing temperature is again indicative of an antiferromagnetic exchange interaction between the two Mn^{IV} ions. This is clearly much weaker than that in **1**, whose $\chi_M T$ drops much more rapidly with

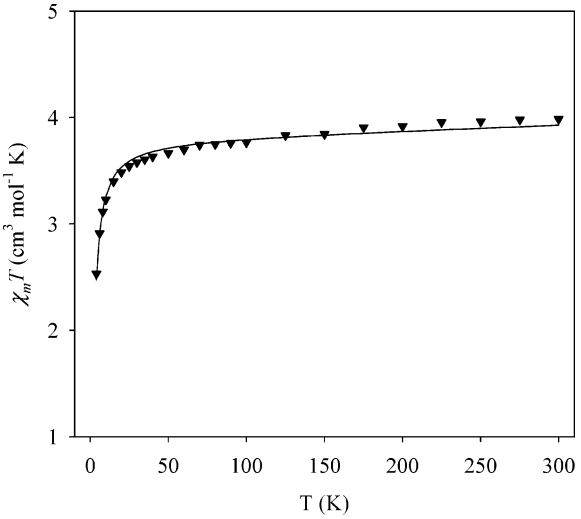

Figure 11. Plot of $\chi_M T$ vs T for complex **4**. The solid line is the fit of the data; see the text for the fit parameters.

temperature, and this is consistent with the greater separation between the two Mn^{IV} ions in **4**. Compounds **5** and **6** show very similar behavior to that of **4**, as expected from their very similar structures. In both cases, the $\chi_M T$ value of 3.95−4.00 cm^3 mol^{-1} K at 300 K decreases slightly to 3.75−3.80 at 100 K and then more rapidly to 2.80−2.90 cm^3 mol^{-1} K at 5.0 K.

All paramagnetism is associated with the Mn^{IV} ions because Ce^{IV} is diamagnetic (f ^{0}). Thus, compounds **1**, **4**, and **5** were treated as dinuclear Mn^{IV}_2 complexes for the purposes of fitting the data to appropriate theoretical expressions. The isotropic (Heisenberg) spin Hamiltonian for a Mn^{IV}_2 dimer is given by eq 6, where J is the exchange interaction parameter and $S_1 = S_2 = 3/2$. This gives a total

$$\mathscr{H} = -2J\,\hat{S}_1\hat{S}_2 \tag{6}$$

of four total spin (S_T) states for the Mn^{IV}_2 complex of S_T = 3, 2, 1, and 0, whose energies $E(S_T)$ are the eigenvalues of the spin Hamiltonian of eq 6 and are given by eq 7. A

$$E(S_T) = -JS_T(S_T + 1) \tag{7}$$

theoretical χ_M versus T equation appropriate for an $S_1 = S_2 = 3/2$ dimer has been previously derived from the use of eqs 6 and 7 and the Van Vleck equation.[21] This expression was modified to include a fraction (p) of paramagnetic impurity (assumed to be mononuclear Mn^{II}) and a temperature-independent paramagnetism (TIP) term, which was held constant at 300 × 10^{-6} cm^3 mol^{-1} K for **1** and 500 × 10^{-6} cm^3 mol^{-1} K for **4** and **5**. Values of 100 × 10^{-6} cm^3 mol^{-1} K per Mn and Ce were employed, which are typical values for these ions.[4a,21b] The resulting theoretical expression was used to fit the experimental data for the three complexes. For complex **1**, the fit of the data is shown as the solid line in Figure 10, and the fit parameters were $J = -45.7(3)$ cm^{-1}, $g = 1.95(5)$, and $p = 0.019$. For complex **4**, the fit is shown

(21) (a) O'Connor, C. J. *Prog. Inorg. Chem.* **1982**, *29*, 203−283. (b) *The Theory of Electric and Magnetic Susceptibilities*; Van Vleck, J. H., Ed.; Oxford University Press: London, 1932.

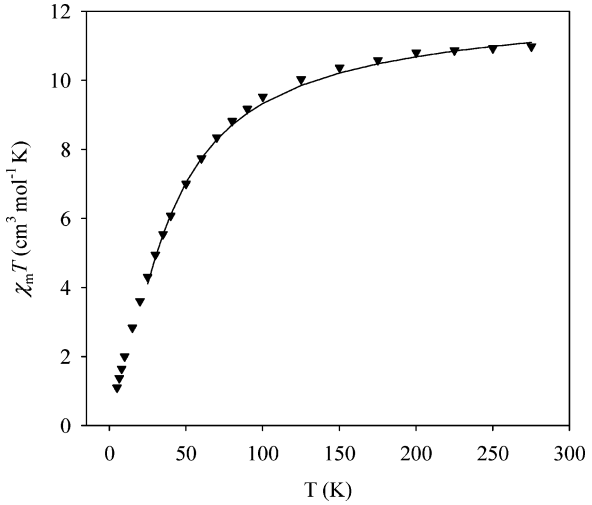

Figure 12. Plot of $\chi_M T$ vs T for complex **3**. The solid line is the fit of the data; see the text for the fit parameters.

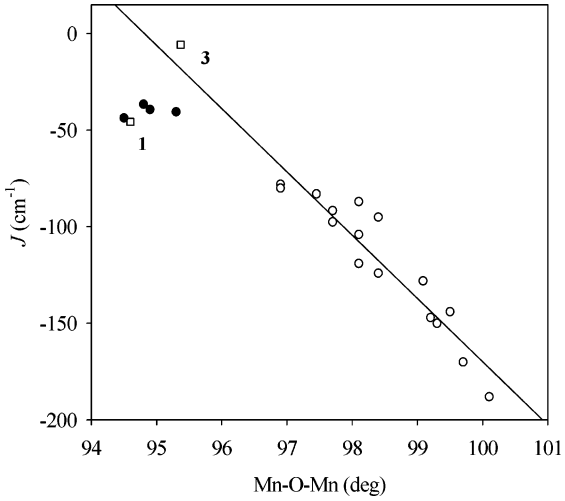

Figure 13. Plot of J vs Mn−O−Mn angle for (○) dinuclear complexes containing the $[Mn^{IV}_2O_2]$ core (adapted from ref 22), (●) dinuclear complexes containing the $[Mn^{IV}_2(\mu\text{-}O)_2(\mu\text{-}O_2CMe)]$ core (adapted from ref 4a), and (□) complexes **1** and **3** from this study.

as the solid line in Figure 11, and the fit parameters were $J = -0.40(10)$ cm^{-1}, $g = 2.0(1)$, and $p = 0.01$. The experimental data for **5** were fit as for **4**, and the fit parameters were essentially identical to those for the latter, being $J = -0.34(10)$ cm^{-1}, $g = 2.0(1)$, and $p = 0.02$.

$\chi_M T$ for $CeMn_6$ compound **3** decreases slowly from 10.88 cm^3 mol^{-1} K at 300 K to 9.52 at 100 K and then more rapidly to 1.1 cm^3 mol^{-1} K at 5.0 K (Figure 12). The 300 K value is slightly lower than the 11.25 cm^3 mol^{-1} K expected for six non-interacting Mn^{IV} centers. The latter and the further decrease with decreasing temperature suggest the presence of dominating antiferromagnetic exchange interactions within **3**. The data were fit by a matrix diagonalization method described elsewhere;[12] only data collected at ≥25 K were employed to avoid the effects of the intermolecular interactions seen in the crystal structure. Four parameters were employed in the fit: J_1 and J_2 for the $\{Mn^{IV}_2O_2(O_2CMe)\}$ and $\{Mn^{IV}_2O(O_2CMe)_2\}$ subunits, respectively; J_3 for a uniform next-nearest-neighbor interaction; and a fraction p of paramagnetic impurity. TIP was kept constant at 700×10^{-6} cm^3 mol^{-1} K. The fit (solid line in Figure 12) gave $J_1 = -5.8(3)$ cm^{-1}, $J_2 = -0.63(10)$ cm^{-1}, $J_3 \approx 0$, $p = 0.029$, and $g = 2.0(1)$. Given that the Mn ions form an even-numbered loop, these antiferromagnetic interactions lead to a ground state spin of $S = 0$ for **3**. The theoretical calculations described below confirm this picture.

Complexes **1**−**6** are thus all antiferromagnetically coupled with S = 0 ground states. Recently, Pecoraro and co-workers reported a linear correlation between the Heisenberg exchange parameter (J) and the mean Mn−O−Mn angle of a number of complexes containing the planar $[Mn^{IV}_2(\mu\text{-}O)_2]$ core.[22] We more recently added to this plot the data points for four compounds containing the $[Mn^{IV}_2(\mu\text{-}O)_2(\mu\text{-}O_2CMe)]$ core, which only roughly follow this trend because their central core is not planar because of the bridging acetate group.[4a] We can now add two additional points, those for complexes **1** and **3**, and present this amended plot in Figure 13. The J value for **1** is in the range expected on the basis of the Mn−O−Mn angles in this pathway and is very close to those for other dinuclear complexes with the $[Mn^{IV}_2(\mu\text{-}O)_2(\mu\text{-}O_2CMe)]$ core, whose Mn_2O_2 central rhomb is slightly bent by the bridging acetate group, as stated above. On the other hand, the J value obtained for the $\{Mn^{IV}_2(\mu\text{-}O)_2(\mu\text{-}O_2CMe)\}$ subunit of **3** (J_2) is significantly weaker than expected for a $[Mn^{IV}_2(\mu\text{-}O)_2(\mu\text{-}O_2CMe)]$ core and, in fact, is essentially that expected for complexes with a planar $[Mn^{IV}_2(\mu\text{-}O)_2]$ core, that is, without the third bridging carboxylate group. We rationalize this as the result of two effects: (A) The attachment of each of the three $\{Mn^{IV}_2(\mu\text{-}O)_2(\mu\text{-}O_2CMe)\}$ subunits of **3** to additional O^{2-} ions and to the central Ce^{4+} ion (see Figure 3) causes the Mn_2O_2 rhomb to be closer to planarity than in the discrete dinuclear complexes such as **1**. This can be quantitated by comparing the closest distance between the Mn−Mn and O−O vectors in the Mn_2O_2 rhomb; it should be zero in the perfectly planar conformation. However, it is 0.218 Å in **1** and 0.125, 0.132, and 0.141 Å for the three subunits in **3**. This is also reflected in the larger dihedral angles within the three $\{Mn_2(\mu\text{-}O)_2\}$ rhombs of **3** (average 169.25°) compared with the 160−165° range in dinuclear complexes with the same $\{Mn^{IV}_2(\mu\text{-}O)_2(\mu\text{-}O_2CMe)\}$ unit.[4a] The closer approach to planarity in **3** means the J value will be weakened relative to discrete complexes with the less planar $[Mn^{IV}_2(\mu\text{-}O)_2(\mu\text{-}O_2CMe)]$ core (Figure 13). (B) The attachment of the $\{Mn^{IV}_2(\mu\text{-}O)_2(\mu\text{-}O_2CMe)\}$ subunits of **3** to the strongly Lewis acidic Ce^{4+} ion (Figure 3) significantly weakens $Mn-O^{2-}$ bonds that mediate the Mn^{IV}_2 superexchange interaction. For example for Mn2 and Mn3 in **2** (Figure 3), the $Mn-O^{2-}$ bonds to μ_3-O atom O3 are significantly longer (Mn2−O3 = 1.868(4) Å, Mn3−O3 = 1.859(4) Å) than those to μ_2-O atom O2 (Mn2−O2 = 1.805(4) Å, Mn3−O2 = 1.819(4) Å). This is, of course, also reflected in the Mn···Mn separations in **2** and **3** (e.g., average 2.714 Å in **3**) compared with the range of 2.58−2.67 Å in dinuclear compounds containing the $[Mn^{IV}_2(\mu\text{-}O)_2(\mu\text{-}O_2CMe)]$ core.[4] The theoretical calculations presented below

(22) Law, N. A.; Kampf, J. W.; Pecoraro, V. L. *Inorg. Chim. Acta* **2000**, *297*, 252.

Table 10. ZILSH Computational Results for Compound **1**

component	ferromagnetic	antiferromagnetic
E (cm^{-1})	393.4	0.0
$2M_1$[a]	3.03	2.99
$2M_2$	3.02	−2.95
$2M_{Ce}$	0.01	0.01
$\langle S_1S_2\rangle$	2.239	−2.164

[a] Two times the *z* component of spin of Mn1, equal to the number of unpaired electrons.

lend support to this suggestion by means of the atomic bond index, which provides a quantitative measure of the bond strengths.

The combined effects of points A and B serve to rationalize the very weak J_1 value for complex **3**. The even smaller J_2 value can also be rationalized on the basis of the long Mn−(μ_3-O^{2-}) bond lengths (1.83 Å) and Mn···Mn separations (3.297 Å), although discrete dinuclear complexes containing the [Mn$^{IV}_2$(μ-O)(μ-O$_2$CMe)$_2$] core are currently unknown and thus unavailable for comparison with the {Mn$^{IV}_2$(μ_3-O)(μ-O$_2$CMe)$_2$} subunit in **3**. Finally, the *J* values for **4** and **5** are also very weak, as expected for two well-separated Mn^{IV} ions interacting through a four-bond superexchange pathway: the Mn···Mn separations in **4** and **5** are 4.818 and 4.792 Å, respectively.

Theoretical Studies. Theoretical calculations were carried out with the ZILSH method[12a] to provide independent estimates of the exchange constants in compounds **1** and **3**. In the former case, the single exchange constant is obtained by computing energies and spin couplings for the ferromagnetic (parallel) and antiferromagnetic (antiparallel) spin components, and then solving eq 1 for *J* and E_0 using eq 8

$$J = \frac{1}{2}\frac{E^{F} - E^{AF}}{\langle S_1S_2\rangle^{AF} - \langle S_1S_2\rangle^{F}} \qquad (8)$$

Results of the calculations on the two spin components are given in Table 10. The *z* components of spin found for each Mn atom ($2M_1$ and $2M_2$ in Table 10) clearly show that each has three unpaired electrons, as appropriate for d^3 Mn^{4+} ions. The Ce^{4+} ion has $M \approx 0$ for both spin components, as expected since Ce^{4+} is diamagnetic. Substitution of the energies and spin couplings of Table 10 into eq 8 gives $J = -44.7$ cm^{-1}, in excellent agreement with the value of −45.7 cm^{-1} obtained from the fit of the magnetization data.

For **3**, results for two components (all Mn spins aligned; spins of Mn_1 and Mn_2 of Figure 3 antiparallel to the others) are given in Table 11. As with **1**, the spin densities clearly show that each Mn atom has three unpaired electrons, as appropriate for d^3 Mn^{4+} ions. The Ce^{4+} ion has no spin density, also as expected. Results for other components are similar. The energy of the component with two spins reversed is lower than that of the component with all spins parallel, indicating the presence of antiferromagnetic interactions within the complex.

Simultaneous solution of the Heisenberg equations for sixteen components (all Mn spins parallel; all possible cases with two spins antiparallel to the others) gives the exchange constants in the middle column of Table 12. The calculations

Table 11. ZILSH Computational Results for Compound **3**

component	ferromagnetic[a]	1, 2 reversed[b]
E (cm^{-1})	200.3	0.0
$2M_1$[c]	3.00	−2.98
$2M_2$	3.00	−2.98
$2M_3$	3.01	3.00
$2M_4$	3.00	3.00
$2M_5$	2.99	2.99
$2M_6$	3.00	2.99
$2M_{Ce}$	0.06	0.02

[a] Component with all metal spins parallel. [b] Component with Mn1 and Mn2 spins antiparallel to the others. [c] Two times the *z* component of spin for Mn1, equal to the number of unpaired electrons.

Table 12. ZILSH Exchange Constants for **3** in the Presence and Absence of the Ce^{4+} Ion

parameter[a,b]	Ce^{4+} present	Ce^{4+} absent[c]
J_{12}	+13.0	+8.3
J_{23}	−9.3	−34.1
J_{34}	+18.0	+13.2
J_{45}	−10.4	−37.4
J_{56}	+15.1	+9.9
J_{16}	−10.1	−37.1

[a] In cm^{-1}, using the numbering scheme of Figure 3. [b] J_{12}, J_{34}, and J_{56} were grouped together as J_2 in the magnetization fit, while J_{23}, J_{45}, and J_{16} were grouped together as J_1. [c] The remaining structure was held fixed.

give alternating antiferromagnetic and ferromagnetic exchange constants, with values of $J_1 \approx -10$ cm^{-1} for the {Mn$^{IV}_2$O$_2$(O$_2$CMe)} bridging units, and $J_2 \approx +15$ cm^{-1} for the {Mn$^{IV}_2$O(O$_2$CMe)$_2$} bridging units. There is good agreement between the J_1 calculated with ZILSH and by fitting the magnetization data (−10 cm^{-1} vs −5.8 cm^{-1}, respectively). Agreement is not as good for J_2, for which the calculations give a positive (ferromagnetic) value. The fit of the magnetization data discussed above showed that all interactions are antiferromagnetic but exhibit the same trend: those for the {Mn$^{IV}_2$O(O$_2$CMe)$_2$} bridging units are less antiferromagnetic/more ferromagnetic than those for the {Mn$^{IV}_2$O$_2$(O$_2$CMe)} units. This shift, and the generally small magnitudes of the exchange interactions in **3**, were attributed above to interactions between the O^{2-} ions bridging the Mn ions with the strongly Lewis-acidic Ce^{4+} ion. The calculations appear to have overestimated this effect. This is not unexpected, however, because the method has previously shown a general tendency to overestimate the ferromagnetic shift caused by stronger field ligands. The complexes [Mn$_2$O(OAc)$_2$Cl$_2$(bpy)$_2$] (**8**) and [Mn$_2$O(O$_2$CPh)$_2$(N$_3$)$_2$(bpy)$_2$] (**9**) provide a good example of this.[23] They have essentially identical metric parameters in their bridging structures (Mn···Mn = 3.152 vs 3.153 Å, Mn−O−Mn = 124 vs 122°, respectively). The only significant difference is in the terminal Cl$^-$ versus N$_3^-$ ligands, which have different ligand field strengths. Fits of magnetic data gave experimental values of $J = -4.1$ cm^{-1} for **8** and $J = +8.8$ cm^{-1} for **9**, clearly showing a shift to ferromagnetic coupling caused by the stronger field azide ligands. ZILSH calculations give $J = -6.8$ cm^{-1} and +29.6 cm^{-1} for **8** and **9**, respectively (see the Supporting Information). As found for **3**, there is very

(23) Vincent, J. B.; Tsai, H. L.; Blackman, A. G.; Wang, S. Y.; Boyd, P. D. W.; Folting, K.; Huffman, J. C.; Lobkovsky, E. B.; Hendrickson, D. N.; Christou, G. *J. Am. Chem. Soc.* **1993**, *115*, 12353.

good agreement between theory and experiment for the exchange constant with weak field ligands (compound **8**), and much poorer agreement for the exchange pathway with stronger field ligands (compound **9**). This shows an apparent tendency of the ZILSH method to overestimate the shift in the ferromagnetic direction in the presence of stronger field ligands. On the basis of these results, it is not surprising that ZILSH would estimate ferromagnetic exchange constants for the $\{Mn^{IV}_2O(O_2CMe)_2\}$ bridging units in **3**.

Despite the predicted ferromagnetic coupling in the $\{Mn^{IV}_2O(O_2CMe)_2\}$ pathway, the ZILSH calculations do predict the correct trend in *J* values for the two pathways in **3**, and provide clear evidence of the effect the Ce^{4+} has on these values. As noted above, the exchange interaction in the $\{Mn^{IV}_2O_2(O_2CMe)\}$ unit ($J_1 = -5.8$ cm^{-1}) is less antiferromagnetic than those found for other known examples of this unit. The interaction in the $\{Mn^{IV}_2O(O_2CMe)_2\}$ unit is even less antiferromagnetic ($J_2 = -0.63$ cm^{-1}). In the preceding discussion, this was attributed to the presence of the strongly Lewis acidic Ce^{4+} ion. This can be directly demonstrated computationally: the effect of the Ce^{4+} ion on the exchange constants was assessed by simply repeated the calculations without the Ce^{4+} ion present, holding the remaining structure constant. The calculated *J* values are now considerably more antiferromagnetic than those found with the Ce^{4+} ion present (Table 12). While a part of the effect of the Ce^{4+} ion is caused by structural changes its presence induces, as suggested above, these results clearly show that the Ce^{4+} ion has a large impact on the exchange constants that is independent of structure.

The effect of the Ce^{4+} ion on the exchange interactions between Mn atoms was rationalized in the previous section as being the result of the Ce−oxide bonding weakening the Mn−oxide bonds which are the primary pathway of these superexchange interactions. Attachment of a Ce^{4+} to a bridging oxide lone pair will have a disproportionate effect on the O^{2-}-to-Mn π-donation that is associated with weaker ligand field strength. A decrease in the O^{2-}-to-Mn π-donation will lower the Mn d_π orbital energies, effectively making the oxide a stronger field ligand with respect to the Mn ions. This would then shift the exchange constant to a less antiferromagnetic/more ferromagnetic value, as discussed above in reference to compounds **8** and **9**.

The proposed changes in bonding strength are clearly reflected in the atomic bond indices computed from the high-spin component (all parallel alignment) wavefunction and shown in Figure 14. The atomic bond index (ABI) represents the strength of bonding interactions, with a value of 1.00 indicating a formal single bond, a value of 2.00 representing a formal double bond, etc. Figure 14 shows two adjacent pathways in **3**, $\{Mn^{IV}_2O(O_2CMe)_2\}$ (Mn1···Mn2) and $\{Mn^{IV}_2O_2(O_2CMe)\}$ (Mn2···Mn3), along with ABI's for all Mn−O bonds in the presence of the Ce^{4+} ion and in its absence (in parentheses in Figure 14). The effect of the Ce^{4+} ion interacting with O1 and O3 is very clear: the ABI for Mn−O^{2-} bonds is reduced by ∼ 0.15 with the Ce^{4+} ion present. This causes the shift in the magnitude of the *J* values, as discussed above.

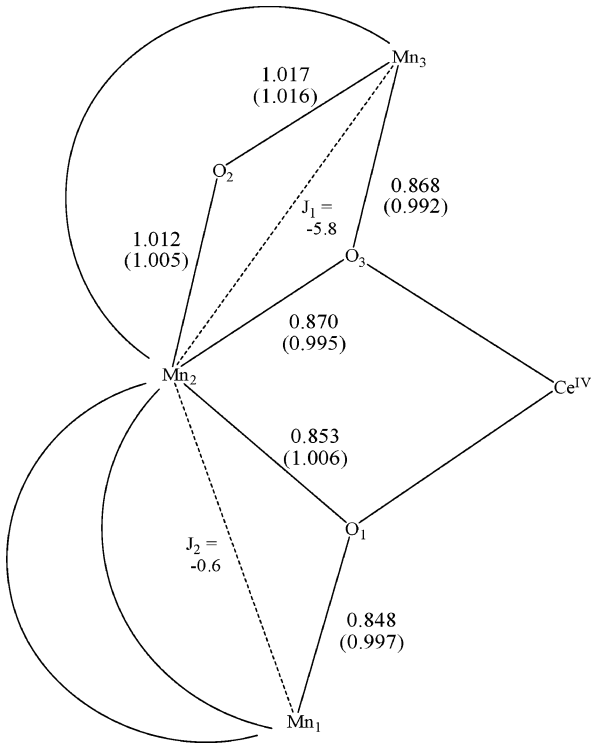

Figure 14. Exchange constants for Mn−Mn interactions (cm^{-1}) and atomic bond indices (ABI) for Mn−O bonds (1.00 = single bond). Values in parentheses were computed with the Ce^{4+} ion omitted and the remaining structure held fixed. Bridging acetate groups are represented by curved lines. Numbering scheme according to Figure 3.

Further support for the role of the Mn−O bonding interactions in shifting the exchange constants to less antiferromagnetic values is given by the correlation between the average ABI and *J* for the two pathways in compound **3**. The average ABI in the $\{Mn^{IV}_2O(O_2CMe)_2\}$ pathway is ∼0.85 with the Ce^{4+} ion present. The $\{Mn^{IV}_2O_2(O_2CMe)\}$ pathway has an additional bridging oxide ligand that does not interact with the cerium ion. The Mn−O interactions with this oxide (O2 in Figure 14) are virtually unchanged by the presence or absence of the cerium ion. The average ABI in this pathway is thus larger in the presence of the cerium ion, ∼0.94. The trend in these values correlates with the trend in *J* values, 0.85/−0.63 versus 0.94/−5.8 cm^{-1} for the $\{Mn^{IV}_2O(O_2CMe)_2\}$ and $\{Mn^{IV}_2O_2(O_2CMe)\}$ pathways, respectively. Together with the results given in the previous paragraph, this provides strong support for the argument that the exchange constants in **3** are less antiferromagnetic than is typical for Mn^{4+}−O−Mn^{4+} exchange pathways because of weakened Mn−O bonding induced by the Lewis acidic Ce^{4+} ion.

Conclusions

The described work has led to the discovery of the first mixed-metal Ce^{IV}/Mn^{IV} complexes. It is somewhat surprising that such species had not been obtained a long time ago given how commonly Ce^{IV} has been used as an oxidizing agent in Mn chemistry. Nevertheless, now that mixed Ce/Mn complexes are known, it has become apparent that there is strong tendency for both metals to be in the high +4 oxidation state. We rationalize this as a synergy resulting from the tendency

of hard Mn^{IV} ions to bind to multiple hard O^{2-} ions, and the tendency of hard O^{2-} ions to stabilize high metal oxidation states such as Ce^{IV}. Although there are a few other reported examples of high oxidation state, mixed transition metal/lanthanide complexes, these contain early transition metal ions such as Ti^{IV} or Nb^{V},[16f] which naturally prefer high oxidation states, in contrast to complexes **1**−**7** in which both component ions are strong oxidizing agents. We recently also reported a $Th^{IV}Mn^{IV}$ complex, a rare high nuclearity mixed 5f/3d complex.[24] However, we do not claim that Mn/Ce complexes will *always* be in the $Ce^{IV}Mn^{IV}$ oxidation state; for example, $[Ce_4Mn_{10}O_{10}(OMe)_6(O_2CPh)_{16}(NO_3)_2(MeOH)_2(H_2O)_2]$ contains $Ce^{IV}_2Ce^{III}_2Mn^{III}_{10}$.[24] It is also interesting that the obtained complexes **1**−**7** span such a wide range of Ce/Mn ratios, and others will undoubtedly be encountered as the work is extended. On a different level, complexes **1**−**7** have unusual and aesthetically pleasing structures, including the first example of a Mn^{IV}_6 wheel. These compounds are also soluble in organic solvents, making them valuable starting materials for further synthesis and reactivity studies. In particular, their solubility, which can be varied by the choice of the carboxylate ligand, in polar and nonpolar organic solvents and the high oxidative strength metal ions they contain might make them candidates as oxidants for a variety of organic and inorganic substrates, perhaps even catalytically.

Magnetic studies have established that the Mn_2 pairwise interactions in all the studied complexes are antiferromagnetic, as expected for Mn^{IV}. However, those in the Ce-centered Mn^{IV}_6 wheel are unusually weak for Mn^{IV}. We have rationalized this, on the basis of structural and computational results, as being caused by the strongly Lewis acidic Ce^{4+} ion and its effect on the $Mn-O^{2-}$ bond lengths, since the bridging O^{2-} ions are the primary pathway of the superexchange interaction between Mn^{IV} centers. Further, comparisons of the results of the computational studies using the ZILSH method with those from the fits of the experimental magnetization data have shown excellent agreement for complex **1** but a systematic ferromagnetic shift of computational versus experimental *J* values for the Ce-centered Mn^{IV}_6 wheel complex **3**. We have again rationalized this as being the result of the Lewis acidic Ce^{4+} ion and its influence on the $Mn-O^{2-}-Mn$ superexchange pathways. Such studies will provide invaluable precedents and guides in the future as the ZILSH method is applied to a variety of other homo- and heteronuclear metal complexes.

Finally, it is clear that heterometallic Ce/Mn chemistry is proving a rich source of new structural types that are unknown or very rare in corresponding homometallic Mn chemistry, and further studies are thus in progress to extend this chemistry as far as possible. These results will be reported in due course.

Acknowledgment. This work was supported by NSF grant CHE-0414555. The theoretical calculations were supported by Shared University Research grants from IBM, Inc., to Indiana University.

Supporting Information Available: X-ray crystallographic data in CIF format for complexes **1**·$2H_2O$, **2**·H_2O·$4MeCO_2H$, **3**·$3H_2O$·$0.5MeCO_2H$, **4**·$2H_2O$, **5**·$2H_2O$·$2MeCO_2H$, and **6**, labeled representations of the molecular and core structure of the cation of **3** (Figures S1 and S2), and ZILSH computational results for compounds **8** and **9** (Table S1). This material is available free of charge via the Internet at http://pubs.acs.org.

IC700994P

(24) (a) Mishra, A.; Abboud, K. A.; Christou, G. *Inorg. Chem.* **2006**, *45*, 2364. (b) Mishra, A.; Tasiopoulos, A. J.; Wernsdorfer, W.; Abboud, K. A.; Christou, G. *Inorg. Chem.* **2007**, *46*, 3105.